

Fernando Ribeiro

**DISPERSÃO DE PLUMAS NO ATLÂNTICO TROPICAL E A
FORMAÇÃO DE BANDAS ZONAIAS DE BAIXA SALINIDADE**

Dissertação submetida ao Programa de Pós-Graduação em Oceanografia, da Universidade Federal de Santa Catarina para obtenção do Grau de Mestre em Oceanografia. Orientador Prof. Dr. Felipe Mendonça Pimenta.

Florianópolis – SC
2017

Ficha de identificação da obra elaborada pelo autor
através do Programa de Geração Automática da Biblioteca Universitária
da UFSC.

Ribeiro, Fernando
DISPERSÃO DE PLUMAS NO ATLÂNTICO TROPICAL E A
FORMAÇÃO DE BANDAS ZONais DE BAIXA SALINIDADE /
Fernando Ribeiro ; orientador, Felipe Mendonça
Pimenta, 2017.
79 p.

Dissertação (mestrado) - Universidade Federal de
Santa Catarina, Centro de Ciências Físicas e
Matemáticas, Programa de Pós-Graduação em
Oceanografia, Florianópolis, 2017.

Inclui referências.

1. Oceanografia. 2. Pluma do Amazonas. 3. Pluma
do Congo. 4. Banda Zonal de Baixa Salinidade. 5.
Reanálise Oceânica. I. Mendonça Pimenta, Felipe. II.
Universidade Federal de Santa Catarina. Programa de
Pós-Graduação em Oceanografia. III. Título.

FERNANDO RIBEIRO

**DISPERSÃO DE PLUMAS NO ATLÂNTICO TROPICAL E A
FORMAÇÃO DE BANDAS ZONAIAS DE BAIXA SALINIDADE**

Florianópolis, 08 de Dezembro de 2017.

Prof.º Dr.º Antônio Henrique da Fontoura Klein
Coordenador do Programa de Pós-Graduação em Oceanografia

Banca Examinadora:

Prof. Dr. Felipe Mendonça Pimenta
Orientador

Prof. Dr. Antonio Fernando Härter Fetter Filho

Prof. Dr. Renato Ramos da Silva

Prof. Dr. Rodrigo do Carmo Barletta
(Membro Externo)

“Os que se encantam com a prática sem a ciência são como os marinheiros que entram no navio sem timão e nem bússola, nunca tendo certeza do seu destino”.

(Leonardo da Vinci)

AGRADECIMENTOS

Eu gostaria de agradecer à minha mãe, Zenir Lucia Ribeiro, por sempre apoiar e ajudar nas minhas decisões, sem ela não seria possível dar mais esse passo acadêmico. Agradeço a minha família em geral, que de uma forma ou outra sempre me deram forças para seguir em frente.

O desenvolvimento desta dissertação foi um período de grande aprendizagem acadêmica e pessoal, onde tive a sorte de ter ao lado um orientador/conselheiro, por isso agradeço profundamente ao meu orientador Felipe Mendonça Pimenta pelas horas de dedicação, paciência e conselhos dados ao longo deste projeto.

Agradeço ao Prof. Dr. Antonio Fernando Härter Fetter Filho pela ajuda com as análises finais deste projeto. Ao Prof. Dr. Denny Kirwan pela rotina de trajetórias lagrangeanas, Peter Brandt pela sugestão dos dados históricos TACE e ao Andrea Storto do Centro Euro-Mediterraneo per i Cambiamenti Climatici (CMCC), Bologna (Italy) pelos dados de reanálise fornecidos. Sou grato ao Coordenador do PPGOCEANO, Prof. Dr. Antônio H. F. Klein, e ao secretário Milano Cavalcante, pelo incentivo e suporte

Agradeço aos companheiros e amigos de laboratório e de curso: Marcus, Bruna, Homero, Laís, Faynna, Fernando, Ana Correa, Cesar, Nassif e Anthea pela companhia e ajuda dada ao longo destes anos.

Finalmente, agradeço à CAPES (Programa: Ciências do Mar II / Edital: 43/2013) Pela bolsa de mestrado concedida durante a execução deste projeto. E aos projetos 486381/2013-7 e 406801/2013-4 pelo apoio à pesquisa.

RESUMO

Este trabalho descreve a variabilidade de plumas derivadas de grandes descargas fluviais do Atlântico Tropical, explorando a importância da precipitação e das correntes oceânicas na manutenção e intrusão destas estruturas. Dados satelitários de salinidade SMOS são combinados com dados hidrográficos históricos e séries temporais das boias PIRATA para comparação com três produtos de modelagem oceânica (OFES, HYCOM e C-GLORS).

A avaliação dos produtos de reanálise ilustra melhor desempenho para o C-GLORS no Atlântico Tropical. O qual foi selecionado para o estudo das plumas.

Seções hidrográficas históricas ilustraram três situações distintas com a formação de camadas superficiais de baixa salinidade. Na seção 44°W, a estrutura observada foi formada pela intrusão da pluma do Amazonas através da Contracorrente Norte Equatorial (NECC), com contribuições significativas de núcleos de precipitação na sua porção distal. Na seção de 35°W as águas de baixa salinidade encontradas foram associadas a um núcleo de precipitação. Por fim, na seção a 28°W, uma cunha de águas relativamente frescas e 75 m de profundidade foi associada a intrusão de águas do Golfo da Guiné, advectadas pelo ramo norte da Corrente Sul Equatorial (nSEC).

A reanálise C-GLORS possibilitou a descrição sazonal e interanual das intrusões da pluma do Amazonas e das águas do Golfo da Guiné relativamente fresca. A intrusão da pluma do Amazonas pela NECC inicia em julho, atingindo uma posição média de 42°W entre outubro e setembro. Já a intrusão de águas frescas da costa Africana atinge a longitude média de 26°W entre maio e outubro.

A variabilidade interanual destas intrusões é significativa e por vezes as plumas geradas na costa Africana e Americana se encontram formando uma única banda zonal de baixa salinidade a 8°N. A banda zonal permanece por cerca de dois meses, possui um período de recorrência de 2 a 6 anos, sendo observada nos anos de 1997, 2000, 2006, 2008, 2011 e 2012. Sua formação não é significativamente correlacionada com a descarga

fluvial ou a precipitação, mas está relacionada à variabilidade do sistema de correntes zonais dirigidas pelo vento.

Keywords: Atlântico Tropical, Rio Amazonas, Contra Corrente Norte Equatorial (NECC), Rio Congo, ramo norte da Corrente Sul Equatorial (nSEC), Zona de Convergência Intertropical, ITCZ.

ABSTRACT

This paper describes the variability of plumes derived from large river discharges of the Tropical Atlantic, exploring the importance of precipitation and ocean currents in the intrusion and maintenance of these structures. Satellite salinity data from SMOS are combined with historical hydrographic data and temporal series of PIRATA buoys for comparison with three oceanic reanalysis products (OFES, HYCOM and C-GLORS). The evaluation of these models suggests a better performance for C-GLORS in the Tropical Atlantic. The correlation with PIRATA buoys is $r=0.98$ for surface temperature and $r=0.95$ for salinity, with a mean squared error (RMSE) smaller than 0.24. The C-GLORS reanalysis was selected for further exploration of oceanographic scenarios it adequately represented the thermohaline structure.

Historical hydrographic sections described three distinct situations with the formation of low salinity superficial layers. At 44°W , the observed structure was formed by the intrusion of Amazon plume through the North Equatorial Countercurrent (NECC), with significant contributions of precipitation on the plume for field.

At 35°W , the low salinity waters detected by ship data was attributed to freshwater derived from precipitation. Finally at 28°W , a fresh water wedge found between 0 and 10°N up to 75 m depth was linked to the intrusion of Gulf of Guinea's river and precipitation waters, advected by the northern branch of the South Equatorial Current (nSEC).

The C-GLORS reanalysis enabled the description of the seasonal and year-to-year variability of the Amazon plume and the Gulf of Guinea's freshwaters intrusions. The intrusion of the Amazon plume by NECC starts in July and reaches the average position of 42°W between October and September. The intrusion of freshwaters from the African coast reaches an average longitude of 26°W between May and October.

The interannual variability of these intrusions is significant and sometimes they meet to form a continuous low salinity zonal band between 4° and 8°N . This band last up to two months, has a return period of 2 to 6 years and has been observed in 1997, 2000, 2006, 2008, 2011 and

2012. Its formation is not significantly correlated to the river discharge or precipitation. The freshwater zonal band formation seems to be attributed to the variability of wind-driven zonal currents.

Keywords: Tropical Atlantic, Amazonas River, North Equatorial Counter-current (NECC), Congo River, South Equatorial Current (nSEC), ITCZ.

SUMÁRIO

1.	Introdução Geral	19
1.1.	Descargas Fluviais	22
1.2.	Sistema de Correntes Equatoriais	24
1.3.	Padrões de precipitação	25
1.4.	Padrões de dispersão das plumas	26
1.5.	Interação Pluma-Atmosfera	30
2.	Justificativa	31
3.	Objetivos	31
3.1.	Geral	31
3.2.	Específicos	31
4.	Hipótese	32
	DISPERSION OF PLUMES IN THE TROPICAL ATLANTIC AND THE FORMATION OF LOW SALINITY ZONAL BANDS	35
	Abstract	35
1.	Introduction	37
2.	Methodology	41
2.1.	Satellite data	42
2.2.	Buoys data	42
2.3.	Hydrographic data	43
2.4.	Ocean model products	43
2.4.1.	HYCOM	44
2.4.2.	OFES	44
2.4.3.	C-GLORS	45
3.	Results	45
3.1.	Satellite data	46

3.2.	PIRATA buoys.....	47
3.3.	Hydrographic profiles.....	51
3.4.	Hydrographic transects and low salinity band formation..	53
3.4.1.	Transect S1 at 44°W.....	53
3.4.2.	Transect S2 at 35°W.....	57
3.4.3.	Transect S3 at 28°W.....	59
3.5.	Seasonal variability.....	63
3.6.	Interannual variability.....	65
4.	Summary and conclusions	68
5.	Acknowledgments	69
6.	References.....	70
5.	CONCLUSÕES E CONSIDERAÇÕES FINAIS.....	75
6.	REFERÊNCIAS	76

FIGURAS DA INTRODUÇÃO GERAL

Figura 1. (A) Salinidade superficial média para o mês de Agosto de 2014 derivada do produto satelitário SMOS, ilustrando a dispersão de descargas fluviais do Atlântico Tropical. Cores representam salinidade superficial com isohalinas de 33.5 e 35. S1, S2 e S3 indicam os transectos hidrográficos TACE explorados neste trabalho (Tabela 1). Boias PIRATA utilizadas estão indicadas por pontos pretos, a boia 8°N, 38°W por um quadrado branco. (B) A descarga dos rios ocorre em uma região de intensas correntes zonais dirigidas pelo vento, indicadas por setas brancas para primavera austral (Stramma, et al., 2009). A Corrente Sul Equatorial (SEC) faz parte do Giro Subtropical do Atlântico Sul. Seu ramo sul (sSEC) dá origem à Subcorrente Norte do Brasil NBUC), que flui ao longo da costa formando a Corrente Norte do Brasil (NBC). Na primavera austral a NBC aumenta seu transporte e inicia o processo de retroflexão (Geyer et al., 1996; Castelão and Johns, 2011). Parte do escoamento segue para o Caribe, outra parte alimenta a Contra Corrente Norte Equatorial (NECC) a 8°N. A NECC faz parte do giro equatorial, formado pela Corrente da Guiné (GC), que contorna a costa Africana no sentido horário (Stramma e Schott, 1999). A parte sul deste giro é formada pelo ramo norte da Corrente Sul Equatorial (nSEC) que flui para oeste à ~4°N. Parte do fluxo da nSEC desiste para oeste retroalimentando a NECC. No painel (B) a média mensal de precipitação derivada do produto ECMWF está ilustrada em cores. Os retângulos mostram as regiões A1, A2 e A3 utilizadas para calcular a precipitação integrada.

..... 21

Figura 2. Figura mostrando o transporte da Corrente Norte do Brasil (NBC), a direção média dos ventos ao longo do ano na região da foz do Rio Amazonas, a vazão média mensal da descarga do Rio Amazonas e a orientação da linha de costa na região do Amazonas. Nota-se que no primeiro semestre do ano ocorre o pico de vazão do Amazonas, os ventos atuam perpendicular à costa e o transporte está baixo. No segundo semestre do ano a descarga do rio Amazonas está

diminuindo, os ventos mudam de direção atuando os alísios de Sudeste, a NBC aumenta seu transporte e ocorre o processo de retroflexão, onde parte do seu fluxo alimenta a NECC. (Adaptado de Nittrouer, 1996).....23

Figura 3. O painel A mostra o padrão de correntes para o período de primavera no hemisfério norte (outono no hemisfério sul). Ainda neste painel percebemos que neste período não há retroflexão da NBC e o giro da guiné encontra-se retraído à costa da África. O painel B ilustra o padrão de correntes para o período de outono no hemisfério norte (primavera no hemisfério sul). Observamos que neste período ocorre a retroflexão da NBC e o giro da guiné se estende para o interior do oceano. (Figuras extraídas de Stramma et al., (1999)).....25

Figura 4. Imagens de satélite mostrando a foz do Rio Congo (painel superior) e a foz do Rio Amazonas (Painel Inferior). Créditos: NASA/USGS.29

Figura 5. Figura mostrando o desvio padrão de salinidade para o mês de agosto de 2013, assim como as principais correntes da região próximo a foz do Rio Congo e Golfo da Guiné: ramo norte da Corrente Sul Equatorial (SEC), Corrente da Angola (AC), Corrente Costeira da Benguela (BCC). (Figura extraída de Chao et al., 2015).30

TABELA INTRODUÇÃO GERAL

Tabela 1. Tabela mostrando as maiores descargas no Atlântico Tropical (Dai and Trenberth, 2002).....22

1. INTRODUÇÃO GERAL

O encontro de águas estuarinas com águas oceânicas frequentemente formam intensos gradientes de densidade e correntes (Garvine, 1999). O desenvolvimento destas estruturas envolve o "espalhamento" de águas estuarinas menos densas sobre águas oceânicas de maior densidade. Por serem flutuantes, tais estruturas formadas pela drenagem continental são comumente chamadas de plumas costeiras (Garvine, 1995). A dinâmica destas feições é controlada pelos ventos, descarga fluvial e correntes ambientais (Lentz and Largier, 2006). Tais forçantes controlam o transporte das águas e também os processos de mistura da pluma com as massas de água circunvizinhas, podendo levar a sua completa dispersão. Plumás alteram a estratificação vertical oceânica, e assim interfem nas trocas de calor e umidade com a atmosfera. Elas também transportam matéria e energia para regiões remotas, as quais não seriam realizadas com facilidade por outros processos oceanográficos.

A estratificação halina causada por plumas pode levar a formação da Camada Barreira (Pailler, 1999). Caracterizada por uma forte píconclina próximo a superfície e que age como um obstáculo, ela inibe as trocas turbulentas da superfície com águas profundas. Como consequência, plumas em superfície podem acumular calor, também apresentando anomalias positivas de temperatura.

A Figura 1a ilustra a média do campo superficial de salinidade para o mês de agosto de 2012, derivados do produto satelitário SMOS (Kerr et al., 2010). Nesta figura é notável a presença de bandas de água fresca próximo à foz de grandes rios como o Rio da Plata (35° S), Amazônicas (0°) e Congo (4° S). Ainda neste painel é possível verificar duas plumas de baixa salinidade direcionadas para o interior do oceano na região Equatorial, onde em alguns pode formar uma única banda de baixa salinidade próximo a 8° N. A Figura 1b ilustra o padrão de precipitação acumulada do mesmo período. Entretanto é difícil aferir a contribuição relativa de cada descarga ou mesmo da precipitação na formação da grande banda de baixa salinidade que atravessa o Atlântico em 8° N. contudo, veremos neste estudo que a formação desta banda zonal não é um

fenômeno isolado e que pode ocorrer periodicamente, com potencial impacto sobre as trocas de calor e presumivelmente o clima.

Diante disso, esta pesquisa buscou contribuir para uma melhor descrição do comportamento e dinâmica de formação desta grande banda zonal de baixa salinidade, investigando como diferentes processos contribuem para sua formação.

O trabalho encontra-se dividido em duas partes principais. A primeira avalia três produtos de reanálise oceânica contra dados satelitários e hidrográficos, a fim de selecionar um produto para a investigação de processos oceanográficos.

Os dados satelitários são derivados da missão SMOS (Kerr et al., 2010), os quais fornecem dados de salinidade e precipitação sobre os oceanos. Os perfis hidrográficos de correntes (ADCP), temperatura e salinidade (CTD) são oriundos de cruzeiros históricos realizados pelo Tropical Atlantic Climate Experiment (TACE). Também são utilizadas séries de salinidade e temperatura coletados através de boias oceanográficas do projeto PIRATA (Bourless et al., 2008).

Os modelos avaliados referem-se ao produto de Reanálise Oceânica do HYCOM (Hybrid Coordinate Ocean Model) (Wallcraft et al., 2009), o OFES (Ocean Global Circulation Model for the Earth Simulator) (Masumoto et al., 2004), e C-GLORS versão 4 (Storto et al., 2016).

A segunda parte da investigação consiste em utilizar os resultados da melhor reanálise oceânica para estudar a dinâmica, a variabilidade sazonal e interanual da banda zonal de baixa salinidade.

Nas próximas seções serão descritos o padrão de vazão dos principais rios do Atlântico, o padrão de precipitação na região equatorial, e as principais correntes equatoriais que direcionam e transportam as águas frescas derivadas dos grandes rios.

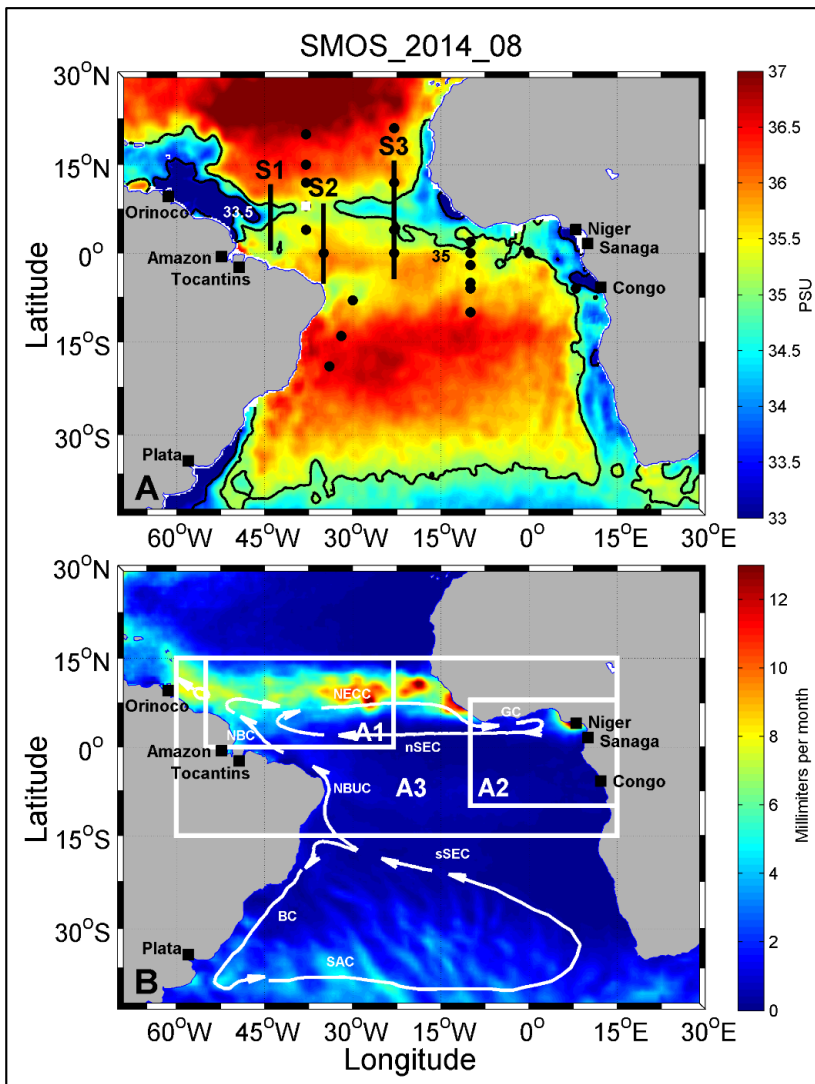


Figura 1. (A) Salinidade superficial média para o mês de Agosto de 2014 derivada do produto satelitário SMOS, ilustrando a dispersão de descargas fluviais do Atlântico Tropical. Cores representam salinidade superficial com isohalinas de 33.5 e 35. S1, S2 e S3 indicam os transectos hidrográficos TACE explorados neste trabalho (Tabela 1). Boias PIRATA uti-

lizadas estão indicadas por pontos pretos, a boia 8°N , 38°W por um quadrado branco. (B) A descarga dos rios ocorre em uma região de intensas correntes zonais dirigidas pelo vento, indicadas por setas brancas para primavera austral (Stramma, et al., 2009). A Corrente Sul Equatorial (SEC) faz parte do Giro Subtropical do Atlântico Sul. Seu ramo sul (sSEC) dá origem à Subcorrente Norte do Brasil NBUC), que flui ao longo da costa formando a Corrente Norte do Brasil (NBC). Na primavera austral a NBC aumenta seu transporte e inicia o processo de retroflexão (Geyer et al., 1996; Castelão and Johns, 2011). Parte do escoamento segue para o Caribe, outra parte alimenta a Contra Corrente Norte Equatorial (NECC) a 8°N . A NECC faz parte do giro equatorial, formado pela Corrente da Guiné (GC), que contorna a costa Africana no sentido horário (Stramma e Schott, 1999). A parte sul deste giro é formada pelo ramo norte da Corrente Sul Equatorial (nSEC) que flui para oeste à $\sim 4^{\circ}\text{N}$. Parte do fluxo da nSEC delete-se para oeste retroalimentando a NECC. No painel (B) a média mensal de precipitação derivada do produto ECMWF está ilustrada em cores. Os retângulos mostram as regiões A1, A2 e A3 utilizadas para calcular a precipitação integrada.

1.1. DESCARGAS FLUVIAIS

O Oceano Atlântico Equatorial é um receptor de grandes descargas fluviais, principalmente na faixa entre 15°N e 15°S . Cinco das maiores descargas de água doce do mundo estão localizada nesta região do oceano e são mostradas na Tabela 1.

Tabela 1. Tabela mostrando as maiores descargas no Atlântico Tropical (Dai and Trenberth, 2002).

Rio	Descarga ($\text{m}^3 \text{s}^{-1}$)
Amazonas/Tocantins	229.994
Zaire	41.082
Orinoco	35.930
Níger	5.769
Sanaga	3.127
Total	235.769

O Rio Amazonas é a maior descarga fluvial do planeta ($229.400 \text{ m}^3 \text{ s}^{-1}$) (Dai and Trenberth, 2002). Sua descarga é superior à soma das próximas seis descargas da lista das maiores do mundo (Pimenta et al., 2011). De acordo com os dados de vazão obtidos na estação de Óbidos-PA, localizada a cerca de 700 km a montante da boca do Rio Amazonas, mostra que este rio tem um pico único de vazão espalhado entre Abril e Julho (Meade et al., 1991; Nittrouer, 1996) e mínima entre outubro e dezembro (Figura 2).

O Rio Congo (Zaire) refere-se a segunda maior vazão do mundo, com aproximadamente $41.100 \text{ m}^3 \text{ s}^{-1}$. Sua máxima vazão ocorre nos meses de novembro e dezembro e a mínima acorre entre junho e agosto (Dai and Trenberth 2002). Sua descarga é responsável por grande variabilidade da salinidade superficial do Golfo da Guiné (Signorini et al. 1999). A terceira maior vazão do mundo é a do Rio Orinoco, com aproximadamente de $36.000 \text{ m}^3 \text{ s}^{-1}$, com grande variabilidade anual (Dai and Trenberth 2002). O pico de vazão ocorre entre agosto e setembro, quando a precipitação sobre a América do Sul se concentra ao norte do Equador (Dai and Trenberth 2002). O Niger e Sanaga possuem menores vazões, apresentadas na Tabela 1.

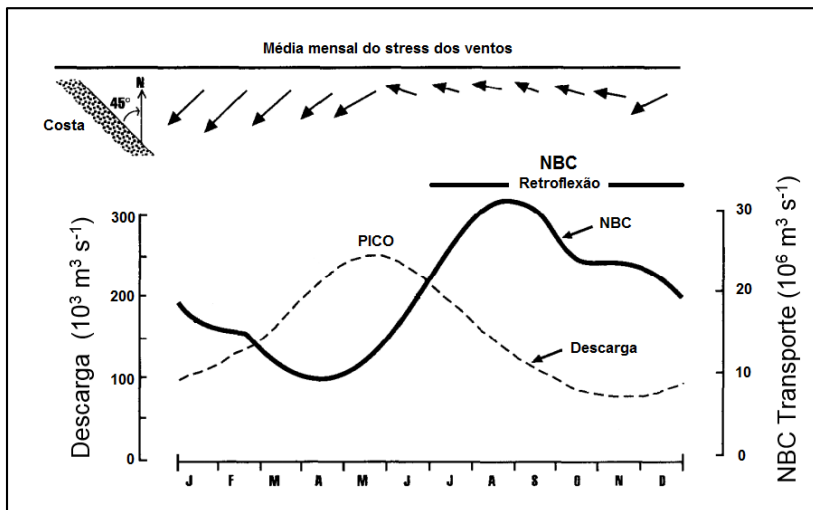


Figura 2. Figura mostrando o transporte da Corrente Norte do Brasil (NBC), a direção média dos ventos ao longo do ano na região da foz do

Rio Amazonas, a vazão média mensal da descarga do Rio Amazonas e a orientação da linha de costa na região do Amazonas. Nota-se que no primeiro semestre do ano ocorre o pico de vazão do Amazonas, os ventos atuam perpendicular à costa e o transporte está baixo. No segundo semestre do ano a descarga do rio Amazonas está diminuindo, os ventos mudam de direção atuando os alísios de Sudeste, a NBC aumenta seu transporte e ocorre o processo de retroflexão, onde parte do seu fluxo alimenta a NECC. (Adaptado de Nittrouer, 1996).

1.2. SISTEMA DE CORRENTES EQUATORIAIS

A descarga dos rios equatoriais ocorrem em uma região de intensas correntes zonais dirigidas pelo vento (Pond and Pickard, 1992). Stramma, et al., (1999) descreveram o sistema de correntes equatoriais para o período de primavera e outono no hemisfério norte, e de maneira geral a Corrente Sul Equatorial, que faz parte do Giro Subtropical do Atlântico Sul (SEC), no seu ramos sul (sSEC) dá origem à Subcorrente Norte do Brasil (NBS). Essa corrente flui ao longo do NE do Brasil e em seguida forma a Corrente Norte do Brasil (NBC) (Figura 3).

A NBC é mais intensa durante a primavera (SON) e verão (DJF) austral (Geyer, 1996; Nittrouer, 1996) (Figura 2). Neste período, a NBC aumenta seu transporte e inicia o processo de retroflexão e emissão de vórtices. Parte do escoamento da NBC segue em direção ao Caribe e outra alimenta a Contracorrente Norte Equatorial (NECC). A NECC é uma corrente zonal dirigida pelo vento que flui aproximadamente ao longo da latitude de 8°N. Ela faz parte de um giro equatorial, formado pela Corrente da Guiné (GC), a qual contorna a costa do Golfo da Guiné, no sentido horário (Figura 3a). O ramo sul deste giro é formado pela Corrente Sul Equatorial no seu ramo Norte (nSEC), que flui aproximadamente à 4°N. Parte do fluxo da nSEC deflete-se para oeste, retroalimentando a NECC e em seguida a GC. Outra parte da nSEC atravessa o Atlântico e segue no sentido ao Caribe, juntando-se a NBC.

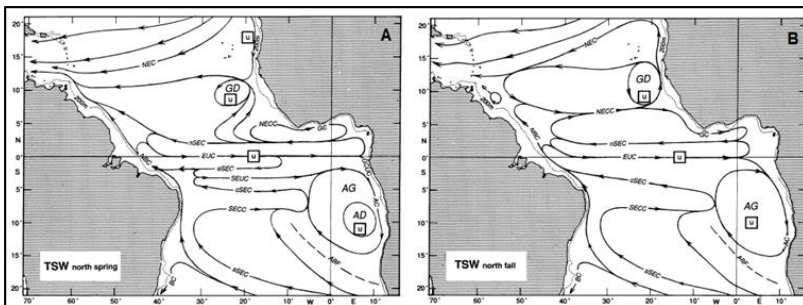


Figura 3. O painel A mostra o padrão de correntes para o período de primavera no hemisfério norte (outono no hemisfério sul). Ainda neste painel percebemos que neste período não há retroflexão da NBC e o giro da guiné encontra-se retraído à costa da África. O painel B ilustra o padrão de correntes para o período de outono no hemisfério norte (primavera no hemisfério sul). Observamos que neste período ocorre a retroflexão da NBC e o giro da guiné se estende para o interior do oceano. (Figuras extraídas de Stramma et al., (1999)).

1.3. PADRÕES DE PRECIPITAÇÃO

A região onde ocorre a formação da banda zonal de baixa salinidade está em uma faixa de latitude de intensa precipitação, devido a Zona de Convergência Intertropical (ICTZ). A ITCZ é considerada o sistema gerador de precipitação mais importante sobre a região equatorial dos oceanos. No Atlântico, ela migra latitudinalmente de 14°N a 2°S e pode ultrapassar essa faixa em alguns anos. Sua posição mais ao norte ocorre nos meses de agosto e setembro e mais ao sul em março e abril (Cavalcante et al., 2009). Sua posição a norte coincide com a intrusão das águas da pluma do Amazonas na NECC. A precipitação integrada na área A3 da Figura 1b é comparável a soma das descargas dos principais rios que desaguam no Atlântico Tropical (Dai and Trenberth 2002).

1.4. PADRÕES DE DISPERSÃO DAS PLUMAS

Duas das maiores vazões de água doce do mundo deságuam no Oceano Atlântico, o Rio Amazonas no Leste e o Rio Congo no Oeste (Figura 1 e Tabela 1). Suas vazões formam extensas plumas de água fresca que espalham-se pelo Atlântico Equatorial (Figura 4). Essas plumas formadas diferem significativamente de plumas formadas nas regiões temperadas e polares. As diferenças primárias são que em baixas latitudes há relativamente alta e estável radiação solar, temperatura, precipitação e escoamento dos rios. Em adição, os ventos são dominados pelos ventos alísios (Nittrouer, 1996).

Um dos primeiros estudos sobre a dispersão da Pluma do Amazonas foi realizado no final da década de 80. Utilizando imagens de satélite (Coastal Zone Color Scanner, CZCS) para monitorar as concentrações de pigmentos fitoplancônicos oriundos da descarga do Rio Amazonas. Muller-Kager et al., (1988) descreveram um padrão de dispersão variável entre o primeiro e o segundo semestre do ano. No primeiro semestre, uma faixa de alta concentração de pigmentos com largura de aproximadamente 150 km ao longo da costa, estende-se da desembocadura do Rio Amazonas até o Caribe. No segundo semestre as águas da pluma são transportadas para a região equatorial do Atlântico.

Lentz, (1995) e Nittrouer, (1996) reuniram dados de direção e intensidade dos ventos, fluxo da NBC, descarga do Rio Amazonas e estações hidrográficas para tentar explicar esse padrão de dispersão. Perceberam que o período de retroflexão da pluma do Amazonas coincidia com o máximo fluxo da NBC, entretanto com lag de dois meses da máxima descarga do Amazonas. Lentz, (1995) identificou a formação de uma piscina de água fresca na boca do Rio Amazonas e atribuíram seu aprisionamento aos intensos ventos alísios de noroeste (perpendicular e contra a foz do Rio Amazonas). Na segunda metade do ano a ITCZ migra para norte e os ventos alísios mudam de direção e a piscina de água fresca é liberada, assim uma grande quantidade de água fresca é advectada pela NBC.

Korosov et al, (2014) combinou os campos de salinidade da missão (Aquarius e SMOS) com imagens de cor do oceano (MODIS), e

desenvolveu um algoritmo baseado em redes neurais para estimar a salinidade do oceano em alta resolução espacial. Seus resultados corroboram aos resultados de Muller-Karger (1988). Coles et al., (2013) estudaram a dispersão da pluma do Amazonas na quebra da plataforma e no oceano aberto utilizando Derivadores Virtuais Lagrangeanos (DVP), simulados com o modelo HYCOM com 1/6 ° de resolução espacial. Seus resultados foram validados com dados coletados por derivadores *in situ*, juntamente com dados da boia PIRATA 8°N, 38°W, e identificando quatro caminhos principais para os derivadores simulados. Sendo dois deles seguindo a direção noroeste. Outros dois seguem para leste junto com a NECC. Os caminhos que seguem para norte são contínuos durante o ano todo, Já os caminhos para oeste são sazonais devido a influência da ITCZ na NECC. Comentam também que a descarga do Rio Amazonas não é uma influência primária na área da pluma ou caminhos que ela seguirá. Resultados do modelo sugerem que águas da pluma do Amazonas chegam a 20°W entre novembro e dezembro. Foster et al., (2009) mostrou que o mesmo nitrogênio fixado com comunidades associadas a Pluma do Rio Amazonas, também foram encontradas junto à água fresca encontrada no Golfo da Guiné, sugerindo conectividade entre as regiões.

A Pluma do Congo foi descrita primeiramente por Eisma and Van Bennekum, (1978), onde descobriram que a pluma é predominantemente orientada para Noroeste, ao invés de seguir para sul, como esperado devido a latitude (6°S) e ao efeito coriolis (Chao et al., 2015). Estudos de modelagem sugerem que a pluma do Congo segue a direção norte, e pode ser explicada pela influência de correntes de densidade devido ao fluxo costeiro, pela geomorfologia do estuário do Congo, correntes oceânicas e pelos ventos (Denamiel et al., 2013; Chao et al., 2015). Durante mais da metade do ano, a pluma estende-se para Noroeste alcançando uma distância da costa entre 400 e 1000 km. Esses autores também sugerem que a pluma é carregada para Noroeste pelas correntes dirigidas pelos ventos, possivelmente o ramo norte da corrente costeira de Benguela (BCC) (Figura 5). A mínima superfície da pluma é alcançada entre Setembro/Outubro, coincidindo com a mínima descarga do Rio Congo e a diminuição dos ventos da região (Hopkins et al., 2013; Chao et al., 2015). Chao et al., (2015) Utilizando dados de salinidade do satélite Aquarius encontrou dois centros de baixa salinidade, um na foz do Rio Congo e

outro ao norte do Equador, no Golfo da Biafra. Mostrou que os dois centros tem alta correlação com a descarga do Rio Congo, porém devido à distância, não está claro que o centro no Golfo da Guiné tenha uma relação direta com a vazão do rio. A foz do Rio Níger fica próximo ao centro de baixa salinidade, contudo sua descarga é uma ordem de grandeza menor que o Congo e é pouco provável que o Rio Níger seja o único a contribuir para sua variabilidade. Berger et al., (2014) encontraram que a precipitação somada a descargas dos pequenos rios poderiam formar a região semi-permanente de baixa salinidade no Golfo da Biafra, Leste do Golfo da Guiné e ao norte do Equador. Já a região de baixa salinidade ao sul do equador foi atribuída diretamente ao Rio Congo (Chao et al., 2015).

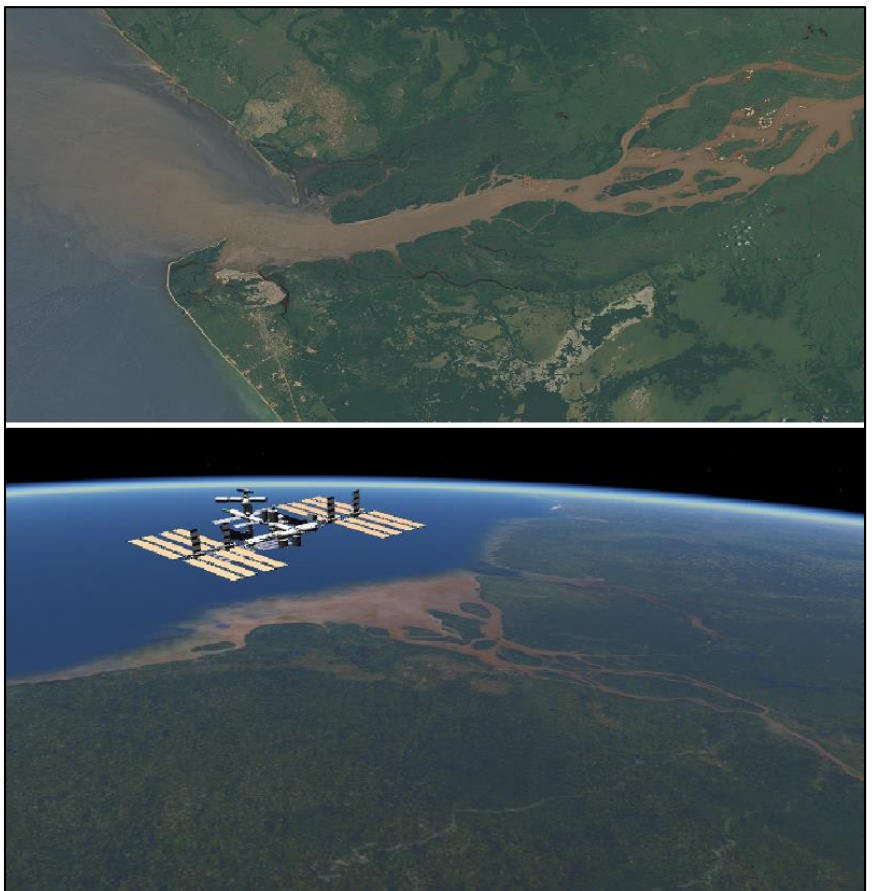


Figura 4. Imagens de satélite mostrando a foz do Rio Congo (painedel superior) e a foz do Rio Amazonas (Painedel Inferior). Créditos: NASA/USGS.

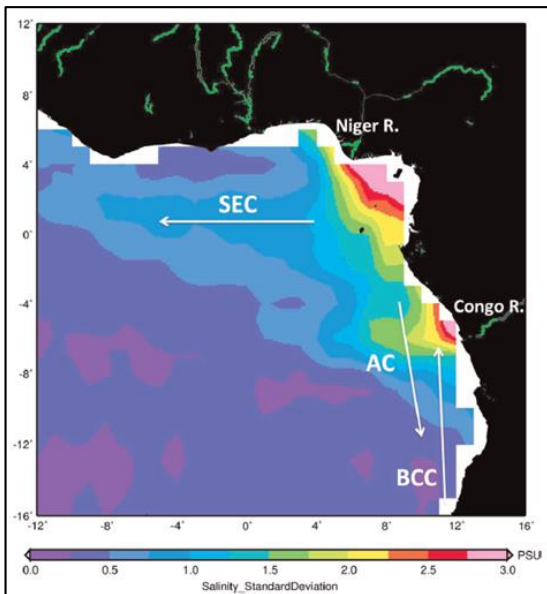


Figura 5. Figura mostrando o desvio padrão de salinidade para o mês de agosto de 2013, assim como as principais correntes da região próximo a foz do Rio Congo e Golfo da Guiné: ramo norte da Corrente Sul Equatorial (SEC), Corrente da Angola (AC), Corrente Costeira da Benguela (BCC). (Figura extraída de Chao et al., 2015).

1.5. INTERAÇÃO PLUMA-ATMOSFERA

As grandes dimensões dessas plumas equatoriais, somada à característica de reter calor, podem sem dúvida causar interferência nos sistemas atmosféricos. Há estudos que sugerem a intensificação de furacões quando estas tempestades tropicais atravessam regiões de águas com baixa salinidade e maior temperatura (Reul et al., 2014; Ffield et al., 2007). Entretanto, ainda há poucos estudos para entender essa interação pluma-atmosfera. Todavia, é notório que essas águas menos salinas e mais quentes estão em uma região berço de furacões e provavelmente intensificando esses sistemas.

2. JUSTIFICATIVA

A dispersão de plumas de grandes rios equatoriais ocorrem de forma complexa e em alguns momentos formam uma única banda de baixa salinidade próximo a latitude de 8°N. Levando em conta que essas bandas de baixa salinidade interferem na variabilidade de sistemas atmosféricos como furacões, este estudo se justifica pela necessidade de conhecer a interação dessas bandas com esses sistemas. Este trabalho, de forma inédita, busca contribuir com a descrição mais detalhada dos mecanismos de formação e variabilidade dessas bandas zonais de baixa salinidade.

3. Objetivos

3.1. GERAL

O presente trabalho tem como objetivo principal investigar a formação de bandas zonais de baixa salinidade no oceano Atlântico Tropical, devido a convergência de águas de menos salinidade oriundas da Pluma do Amazonas e do Giro da Guiné.

3.2. ESPECÍFICOS

Objetivos específicos são:

- (1) Avaliar a performance de três produtos de modelagem oceânica HYCOM, OFES e C - GLORS baseado nos dados de boias do projeto (PIRATA), hidrografia (Tropical Atlantic Climate Experiment – Geomar) e satélite (SMOS);

- (2) Descrever a formação da grande banda de baixa salinidade do oceano Atlântico Equatorial;

- (3) Calcular a trajetória de derivadores superficiais virtuais para avaliar a dispersão das águas do Rio Amazonas, e contribuição da precipitação na manutenção da pluma.
- (4) Descrever a variação sazonal e interanual da formação da Banda Zonal de Baixa Salinidade.

4. HIPÓTESE

- (1) A hipótese dessa investigação é a formação de Bandas Zonais de Baixa Salinidade no oceano tropical controladas dominante-mente pelo sistema de correntes equatoriais;
- (2) No seu campo distante a pluma do amazonas é alimentada pela precipitação da Zona de Convergência Intertropical (ZCIT), que permite manter uma estrutura zonal de baixa salinidade e forte estratificação vertical, ajudando assim na formação e manuten-ção de Bandas Zonais de Baixa Salinidade.

DISPERSION OF PLUMES IN THE TROPICAL ATLANTIC AND THE FORMATION OF LOW SALINITY ZONAL BANDS

Este capítulo apresenta o artigo que compõe esta dissertação e que foi submetido à revista Deep-Sea Research Part I: Oceanographic Research Papers em 17/11/2017. O conteúdo apresentado a seguir segue na íntegra o submetido à revista. A confirmação da submissão é apresentada na próxima página.

Successfully received: submission DISPERSION OF PLUMES IN THE TROPICAL ATLANTIC AND THE FORMATION OF LOW SALINITY ZONAL BANDS for Deep-Sea Research Part I

Deep-Sea Research Part I <EvideSupport@elsevier.com>
Reply-To: dsn@elsevier.com
To: fernandolageano@gmail.com

Fri, Nov 17, 2017 at 3:28 PM

This message was sent automatically. Please do not reply.

Ref: DSR1_2017_281

Title: DISPERSION OF PLUMES IN THE TROPICAL ATLANTIC AND THE FORMATION OF LOW SALINITY ZONAL BANDS

Journal: Deep-Sea Research Part I

Dear Mr. Ribeiro,

Thank you for submitting your manuscript for consideration for publication in Deep-Sea Research Part I. Your submission was received in good order.

To track the status of your manuscript, please log into EVISE® at: http://www.evise.com/evise/faces/pages/navigation/NavController.jsp?JRNL_ACR=DSR1 and locate your submission under the header 'My Submissions with Journal' on your 'My Author Tasks' view.

Thank you for submitting your work to this journal.

Kind regards,

Deep-Sea Research Part I

Have questions or need assistance?

For further assistance, please visit our [Customer Support](#) site. Here you can search for solutions on a range of topics, find answers to frequently asked questions, and learn more about EVISE® via interactive tutorials. You can also talk 24/5 to our customer support team by phone and 24/7 by live chat and email.

Copyright © 2017 Elsevier B.V. | [Privacy Policy](#)

[Elsevier B.V.](#), Radarweg 29, 1043 NX Amsterdam, The Netherlands, Reg. No. 33156677.

DISPERSION OF PLUMES IN THE TROPICAL ATLANTIC AND THE FORMATION OF LOW SALINITY ZONAL BANDS

Fernando Ribeiro, Felipe M. Pimenta, Antonio Fetter

Graduate Program of Oceanography. Center for Mathematics and Physics Sciences.

Federal University of Santa Catarina, Florianópolis, SC, 88010-970, Brazil.

Abstract

This paper describes the variability of plumes derived from large river discharges of the Tropical Atlantic, exploring the importance of precipitation and ocean currents in the intrusion and maintenance of these structures. Satellite salinity data from SMOS are combined with historical hydrographic data and temporal series of PIRATA buoys for comparison with three oceanic reanalysis products (OFES, HYCOM and C-GLORS). The evaluation of these models suggests a better performance for C-GLORS in the Tropical Atlantic. The correlation with PIRATA buoys is $r=0.98$ for surface temperature and $r=0.95$ for salinity, with a mean squared error (RMSE) smaller than 0.24. The C-GLORS reanalysis was selected for further exploration of oceanographic scenarios it adequately represented the thermohaline structure.

Historical hydrographic sections described three distinct situations with the formation of low salinity superficial layers. At 44°W , the observed structure was formed by the intrusion of Amazon plume through the North Equatorial Countercurrent (NECC), with significant contributions of precipitation on the plume for field.

At 35°W , the low salinity waters detected by ship data was attributed to freshwater derived from precipitation. Finally at 28°W , a fresh water wedge found between 0 and 10°N up to 75 m depth was linked to the intrusion of Gulf of Guinea's river and precipitation waters, advected by the northern branch of the South Equatorial Current (nSEC).

The C-GLORS reanalysis enabled the description of the seasonal and year-to-year variability of the Amazon plume and the Gulf of Guinea's freshwaters intrusions. The intrusion of the Amazon plume by NECC starts in July and reaches the average position of 42°W between October and September. The intrusion of freshwaters from the African coast reaches an average longitude of 26°W between May and October.

The interannual variability of these intrusions is significant and sometimes they meet to form a continuous low salinity zonal band between 4° and 8°N. This band last up to two months, has a return period of 2 to 6 years and has been observed in 1997, 2000, 2006, 2008, 2011 and 2012. Its formation is not significantly correlated to the river discharge or precipitation. The freshwater zonal band formation seems to be attributed to the variability of wind-driven zonal currents.

Keywords: Tropical Atlantic, Amazon River, North Equatorial, Counter-current (NECC), Congo River, South Equatorial Current (nSEC), ITCZ.

1. INTRODUCTION

The meeting of rivers with the sea typically forms coastal plumes, structures characterized by less dense waters derived from continental drainage which spread over saltier and denser waters of the oceanic region (Garvine, 1995). The dynamics and dispersion of plumes rely on diverse factors, such as the magnitude of the discharge, the latitude, the bathymetry and other oceanographic drivers such as winds, tides and ambient currents (Garvine, 1999; Fong and Geyer, 2001; Lentz, 2004; Pimenta et al., 2011).

In average and high latitudes, large discharges tend to form plumes influenced by the earth's rotation that can form a coastal bulb at the mouth of the estuary. More generally, however, these discharges form a coastal plume along the coast that propagates in the direction of a Kelvin wave, leaving the coast to the right (left) in the northern (southern) hemisphere (Garvine, 1995; Yankovsky and Chapman, 1997; Fong and Geyer, 2002; Lentz and Largier, 2006; Whitney and Garvine, 2005; Pimenta et al., 2011; Palma and Matano, 2017).

In low latitudes, large discharges tend to form superficial plumes which convey fresh water preferentially to the open ocean. On the eastern borders of ocean basins, the discharges are characterized by the emission of fresh water eddies which propagate to the west. On the western shores, the theory predicts plumes parallel to the coast that tend to deflect and intrude along the equatorial region (Palma and Matano, 2017).

The Tropical Atlantic is singular as it receives the input of the three largest river discharges of the world in low latitudes: Amazon and Tocantins River ($229400 \text{ m}^3 \text{ s}^{-1}$), Congo River (Zaire) ($41100 \text{ m}^3 \text{ s}^{-1}$) and the Orinoco ($34900 \text{ m}^3 \text{ s}^{-1}$) (Hovius, 1998; Dai and Trenberth, 2002). The magnitude of these discharges is so significant that their impact over the ocean can be observed from the space and far away from the coast (Figure 1). The surface salinity field shown is derived from the SMOS satellite (Kerr et al., 2010) and illustrates the presence of fresh waters around the mouths of Amazon and Tocantins (0°), Orinoco (2°N), Congo (6°S), Sanaga (3.5°N) and Niger (5°N) rivers in August of 2014. It is also possible to observe the plume of the Plata River (35°S) and the accumulation of fresh waters in the Gulf of Guinea (0°N , 5°E).

Figure 1b shows the pattern of precipitation accumulated during the same period when the Intertropical Convergence Zone (ITCZ) is in its northern position (Cavalcanti et al., 2009). As we will discuss, the contribution of the oceanic precipitation integrated between 15°N e 15°S has a comparable magnitude to the discharge of the mentioned rivers altogether.

Muller-Karger et al. (1988), Lentz and Limeburner (1995), Coles et al. (2013) and Korosov et al. (2015) described the intrusion and dispersion patterns of the Amazon plume in the Tropical Atlantic. During the first semester, its freshwaters follows the northeast path to the Caribbean Sea along with Orinoco river waters. From the second semester on, the transport of North Brazil Current (NBC) increases and starts its retroflection, injecting the Amazon plume into the Tropical Atlantic through the North Equatorial Countercurrent (NECC) (Geyer et al., 1996; Korosov et al., 2015; Castelão and Johns, 2011) (Figure 1a,b).

Eisma and Van Bennekom (1978) describe the Congo plume as predominantly oriented to the northeast. Other studies showed that its extension reaches from 400 to 1000 km from the coast, supposedly controlled by winds and by the northern portion of the Benguela Current (Denamiel et al., 2013).

Chao et al. (2015) described two low salinity centers of the African coast: the first near the mouth of the Congo River and the other north of the Equator, in the Gulf of Guinea. Berger et al. (2014) suggest that the precipitation along with the rivers' discharges forms a semi-permanent low salinity region on the Gulf of Guinea (Figure 1a).

These different freshwater sources impact the ocean vertical stratification, influencing mixing and potentially altering exchange processes of heat and humidity with the atmosphere. The interaction of plumes with the large-scale current system enables the efficient transport of freshwaters to remote regions, which would not be possible by other oceanographic processes.

In the Tropical Atlantic, the stratification induced by the plumes and precipitation can lead to the formation of a barrier layer, char-

acterized as the region between a shallow halocline and a deeper thermocline (Pailler et al., 1999). The halocline inhibits turbulent mixing, accumulating surface heat and impacting atmospheric and climatic processes. Reul et al. (2014), Ffield (2007) e Balaguru et al. (2012) found a strong relationship between the intensification of the hurricanes, the position of the hot and shallow layer of the barrier layer and the plumes of the Amazon and Orinoco rivers.

Ahead of these factors, this research contributes to a better description of the variability of low latitude plumes in the Tropical Atlantic, with emphasis on the dispersion of the Amazon River and the Gulf of Guinea's fresh waters. As we will see further, the ocean large-scale circulation plays a fundamental role in the spatial dispersion of these plumes which come to form a low salinity zonal band.

For this purpose, this paper combines the analysis of satellite data from the SMOS mission (Kerr et al., 2010), with historical hydrographic data from the TACE program (Tropical Atlantic Climate Experiment), temporal series of oceanic buoys from the PIRATA program (Bourlès et al., 2008), and three model products selected for evaluation. The models products refer to the HYCOM (Hybrid Coordinate Ocean Model) (Wallcraft et al., 2009), OFES (Ocean Global Circulation Model for the Earth Simulator) (Masumoto et al., 2004) and C-GLORS version 4 (Centre for Climate Change Global Ocean Reanalysis System) (Storto et al., 2016).

The results of this article are divided into two principal parts. In the first part, the ocean reanalysis are compared to satellite data, temporal series of PIRATA and the hydrographic data, in order to select a product for the investigation of the oceanographic processes. In the second part, the combined set of information is used to describe the formation of the superficial low salinity layers detected in the hydrographic data. The dynamics of freshwater formed in the African and South American coasts is explored, estimating the importance of the river discharge, precipitation and currents in the seasonal and interannual variability of low salinity zonal bands.

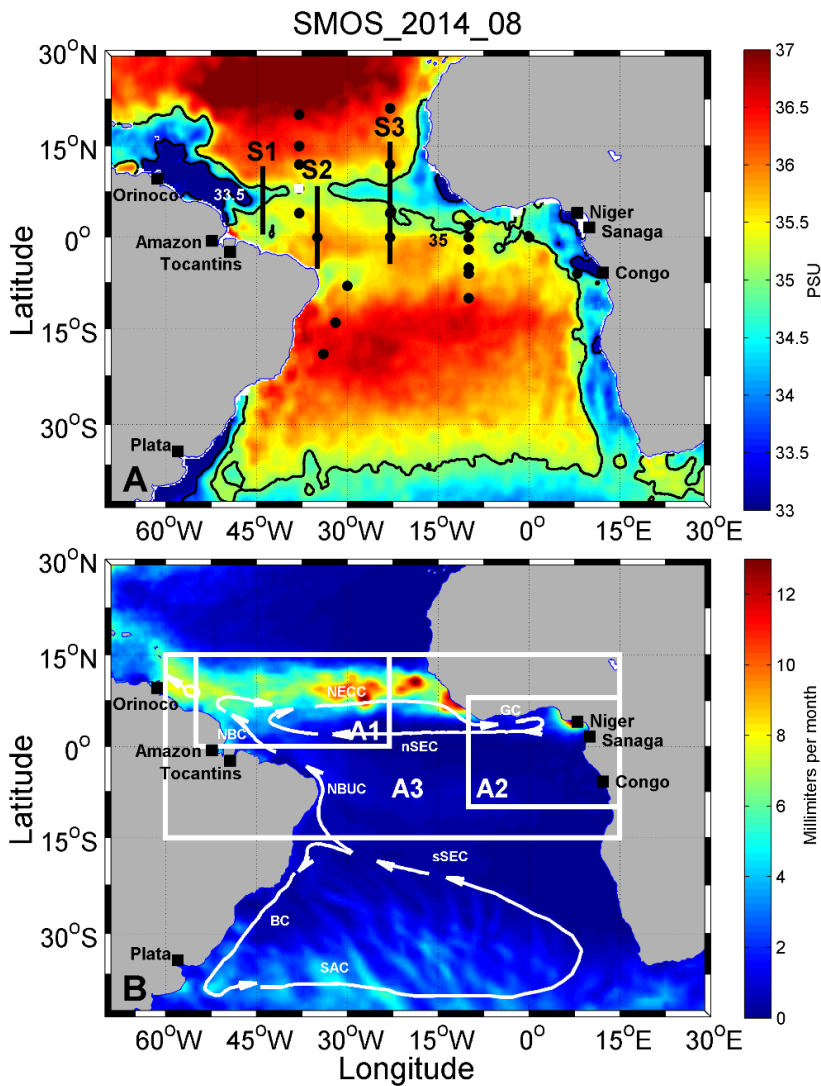


Figure 1. (A) Average surface salinity from the SMOS satellite product for August 2014, illustrating the dispersion of river discharges of the Tropical Atlantic. Colors represent the surface salinity with isolines of 33.5 and 35. S1, S2 and S3 indicate the hydrographic transects from

TACE explored in this paper (Table 1). PIRATA buoys are indicated by black dots, the buoy 8°N, 38°W by a white square. (B) The river discharge occurs in a region of intense wind-driven zonal currents, indicated by white arrows for the southern spring (Stramma et al., 2009). The South Equatorial Current (SEC) is part of the South Atlantic Subtropical Gyre. Its southern side (sSEC) leads to the North Brazil undercurrent (NBUC) which flows along the coast forming the North Brazil Current (NBC) (Schott et al., 2005). During the southern spring, the NBC transport increases and starts its retroflexion (Geyer et al., 1996; Castelão and Johns, 2011). Part of the discharge follows to the Caribbean, the other part feeds the North Equatorial Countercurrent (NECC) at 8°N. The NECC is part of the equatorial gyre, formed by the Guinea Current (GC) which circumvents the African coast in a clockwise rotation (Stramma and Schott, 1999). The southern part of the gyre is formed by the northern branch of the South Equatorial Current (nSEC) which flows west at 4°N. Part of the nSEC deflects to the east merging with the NECC. In the panel (B), the monthly average derived from ECMWF is illustrated in colours. The rectangles show the regions A1, A2 and A3 used to calculate the integrated precipitation.

2. METHODOLOGY

The absence of long time series and the difficulty of covering large hydrographic distances in short times often poses a difficult to the investigation of large scale phenomena. In order to circumvent this problem, the information from satellite products, historical hydrographic data, PIRATA buoys time series and ocean reanalysis products are combined. The remote salinity data help to evaluate the quality of the ocean reanalysis products. Hydrographic data enable the vertical structure description of the plume, also evaluating the efficiency of the models. The reanalysis dataset enabled the investigation of plumes variability and the influence of the precipitation in the formation of low salinity layers. Figure 2 shows the coverage of the datasets used in this study.

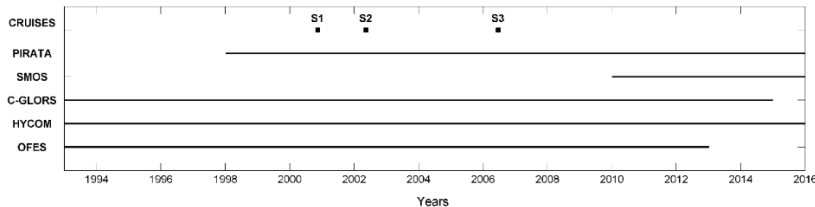


Figure 2. Period of coverage of the satellite temporal series (SMOS), re-analysis (C-GLORS, HYCOM and OFES), buoys (PIRATA) and hydrographic cruises S1, S2 and S3 (cruises) used in this paper.

2.1. Satellite data

The SMOS (Soil Moisture and Ocean Salinity) is a mission from the European Spatial Agency (ESA) aimed to supply global maps of soil humidity and sea surface salinity. Launched in November of 2009, the orbital platform transmits continuous data which are regularly received at the Villafranca station in Spain. Its main sensor is the Microwave Imaging Radiometer using Aperture Synthesis (MIRAS) and consists of a three-arm antenna of 4.5 meters. On these arms 69 elements named LICEF are distributed. Each element receives the radiation emitted from the Earth on the L band (1400-1427 MHz). This radiation is then amplified and stored (Kerr et al., 2010). Here the product SMOS L3 has been selected, with a spatial resolution of $1/4^\circ$ (around 27 km). Monthly averages have been used for the spatial comparison of the superficial fields and averages of three days for the comparison of temporal series.

2.2. Buoys data

The PIRATA program (Prediction and Research Moored Array in the Tropical Atlantic) has been developed by NOAA (National Oceanic and Atmospheric Administration) of the United States in partnership with France and Brazil. The program consists of a system that aims the collection, quality control and operational data distribution for monitoring of oceanographic and climatic processes (Bourlès et al., 2008). The buoys have surface winds sensors, temperature and salinity in the water column and other atmospheric parameters. Here 21 buoys have been selected for

study of the tropical region, as indicated by Figure 1. The PIRATA data was used to access the performance of the models' products.

2.3. Hydrographic data

Hydrographic data was obtained by historical cruises of the Meteor ship conducted in the Atlantic Ocean and provided by the TACE program (Tropical Atlantic Climate Experiment). A total of three meridional transects at the longitudes of 44°W, 35°W e 28°W are used, covering distinct situations when surface low salinity layers were detected. A total of 104 CTD vertical profiles were analysed. The oceanographic transects refer to the cruise M151 of November 2000, M53 of May 2002 and M68 of June 2006, respectively illustrated by S1, S2 and S3 in Figure 1a and listed on Table 1.

Table 1. Meridional transects S1, S2 and S3 with the identification of the hydrographic cruises, period of sampling, number of CTD profiles used and geographical position. Source: Tropical Atlantic Climate Experiment (<http://tace.geomar.de/data/cuisedata/index.html>).

Transect	Cruises	date	Number Of profiles	Latitude	longitude
S1	M151	10/11 to 14/11/2000	20	00.74°N to 11.77°N	44°W
S2	M53	09/05 to 15/05/2002	35	04.74°N to 07.90°N	35°W
S3	M68	16/06 to 07/07/2006	49	03.99°N to 15.31°N	28°W

2.4. Ocean model products

Hereinafter the three products of oceanic reanalysis evaluated in this paper are presented.

2.4.1. HYCOM

The HYCOM reanalysis project (Hybrid Coordinate Ocean Model)¹ is a multinational effort sponsored by the NOPP (National Ocean Partnership Program) as part of GODAE (US Global Ocean Data Assimilation Experiment) aimed to develop and evaluate an oceanic model with data assimilation. Among the main objectives are the representation of the ocean three-dimensional state in high spatial and real-time resolution, the provision of boundary conditions for coastal and regional models, as well as a global coupled ocean-atmosphere forecast model. The system includes sophisticated techniques for the assimilation of satellite sea surface topography and temperature, as well as *in-situ* temperature and salinity data. Its results are available in the spatial resolution of $1/12^\circ$ (~ 9 km) in 40 vertical levels and daily temporal resolution. The available data cover the period from 1992 up to the present. The climatological discharge of HYCOM is implemented in the form of surface virtual salt flux in the river mouth (Wallcraft et al., 2009). HYCOM also employs a barotropic pressure term to mimic the presence of the river and a parameterization for salt vertical mixing (Schiller and Kourafalou, 2010).

2.4.2. OFES

OFES, the OGCM (Ocean Global Circulation Model) for the Earth Simulator is a product based on the Modular Ocean Model (MOM3) developed by the Geophysical Fluid Dynamics Laboratory (GFDL/NOAA). The domain covers the region from 75°N to 75°S , with a horizontal spatial resolution of $1/10^\circ$ and 54 vertical levels (Masumoto et al., 2004). OFES uses the wind climatology and precipitation from NCEP (Kalnay et al., 1996). Heat fluxes are calculated following Rosati and Miyakoda (1988) with monthly variables of atmospheric reanalysis. Monthly salinity data from the World Ocean Atlas 1998 (WOA98) were used to start the model and to compute the salinity restoring fluxes that lead to climatological convergence of the surface salinity fields. OFES does not perform any ocean data assimilation during the model integration. The river discharge is inserted as surface fresh water flux that is spa-

¹ <https://hycom.org>

tially distributed in the region near the estuary. Additional parameterizations provide vertical mixture of fresh water near the rivers' mouths (Pacanovsky and Griffies, 1999).

2.4.3. *C-GLORS*

The C-GLORS version 4 refers to a model of the Euro-Mediterranean Center for Climate Change (CMCC) called CMCC Global Ocean Reanalysis System (C-GLORS) (Storto et al., 2016). The reanalysis covers the period of 1982-2014. The model of ocean general circulation used in the reanalysis C-GLORS is the Nucleus for European Modeling of the Ocean (NEMO) version 3.2.1 (Madec et al., 1998). The reanalysis has a resolution of $1/4^\circ$ in the equator, with a grid ranging from 10 km in high latitude to 27 km in the equator, and 50 vertical levels. Main atmospheric forcings are derived from the Large and Yeager (2004) dataset. Precipitation fields are obtained from the ERA-Interim atmospheric reanalysis and corrected with a climatological coefficient from the Remote Sensing Systems/Passive Microwave Water Cycle (REMSS/PMWCC), as described by Storto et al. (2012). River discharges are implemented as monthly climatological averages from Dai and Trenberth (2002), also spatially distributed near the estuaries' mouths. The C-GLORS uses a 3D variational analysis system (3DVAR), originally formulated for the Mediterranean Sea (Dobricic and Pinardi, 2008) and adapted for the global ocean (Storto et al., 2011). The system, called OceanVar, assimilates in situ observations of temperature, salinity and of sea surface topography. The observations obtained from buoys, Argo floaters, XBTs and CTDs are provided by the ENSEMBLES EN3v2a dataset (Ingleby and Huddleston, 2007).

3. RESULTS

Results are organized in six subsections. The first three describe results of the comparison of ocean models with satellite data, ocean buoys and hydrographical profiles in the Tropical Atlantic. The next subsections explore the oceanographic scenarios registered by the historical hydrographic transects, describing the role of precipitation and river discharge in the formation of low salinity surface layers. Finally, the mechanism for

the formation of low salinity zonal bands is described, as well as its seasonal and year-to-year variability.

3.1. Satellite data

Figure 3 compares the average fields of surface salinity derived from SMOS mission with three ocean modeling products (OFES, HYCOM and C-GLORS) for Setember 2012. Figure 3a, derived from SMOS, depicts the intrusion of the Amazon plume along the latitude 8°N. The surface salinity field also indicate the formation of a low salinity zonal band which crosses the Atlantic Ocean from the South American coast to Africa, between latitudes 3°N and 10°N. The Orinoco plume, located at 10°N is displaced to the northeast and partially fused with the Amazon plumes' waters. A fresh water band is observed along the entire African coast, including the Gulf of Guinea. It is also possible to see the coastal intrusion of fresh waters from the Rio de la Plata between 35° and 28°S. It is difficult, however, to evaluate the contribution of the continental discharge to surface salinity in contrast to the precipitation.

The panels of Figure 3b, c and d represent the monthly averages from the reanalysis products for the same period. OFES (Figure 3b) does not faithfully represent the observed salinity data. The numerically simulated amazon plume display a shorter extension and the low salinity zonal band is absent from the results of this model. HYCOM (Figure 3c) does not form the Amazon plume intrusion into the Tropical Atlantic. In the results of this model, the plume flows along the continental shelf towards the Caribbean Sea. According to the observations HYCOM shows a low salinity signal in the east of the Atlantic but it does not form the low salinity zonal band nor represent the real extension of the Plata plume, that is limited to 32°S. The model product which compares more favorably to the SMOS data is C-GLORS (Figure 3d). This model satisfactorily reproduces the Orinoco's plume, the NBC retroflection and the intrusion of the Amazon plume in the Tropical Atlantic, as well as the formation of low salinity zonal band. The C-GLORS also represents the accumulation of fresh waters in the Gulf of Guinea and Rio de la Plata plume but does not reproduce the entire coastal band of low salinity waters found southwest of the African continent.

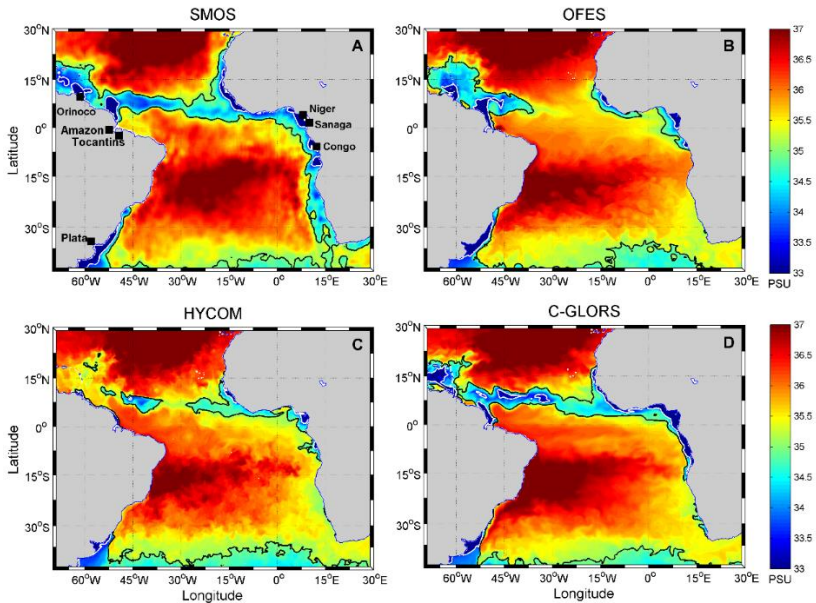


Figure 3. Surface salinity field derived from SMOS satellite product for September 2012. The average fields derived from ocean models for the same period are indicated. In each panel, the salinity is represented by colors. Isohalines of 33.5 and 35 PSU are indicated by white and black lines respectively.

3.2. PIRATA buoys

After a first evaluation of the surface salinity fields, we compared the model and SMOS results to the temporal series derived from PIRATA ocean buoys. Figure 4 compares the surface salinity time series of the PIRATA buoy 8°N 38°W, with SMOS data and three model products, displayed in three different panels. PIRATA observations, illustrated by blue dots, describe seasonal variations that are generally between 36 and 34 PSU but with salinity drops, sometimes reaching 31 PSU. This signal refers mostly to the intrusion of the Amazon plume by NECC at 8°N, which happens preferentially between August and November. Comparing PIRATA with the satellite data, illustrated by red dots, it is possible to observe that SMOS follows the main tendency of the in-situ data, but

sometimes over-estimate the salinity minimum, with differences up to 1 PSU.

Data derived from the model products are indicated by gray lines in each panel. OFES (upper panel) does not represent the observed minimum of salinity, particularly for 2008, 2009 and 2010. The differences in these three periods reach 4 PSU. The second panel illustrates the temporal series of HYCOM, which does not represent the real amplitude of the low salinity pulses. The C-GLORS reanalysis stands out as it more faithfully represents the salinity variability.

The following Figure 5, 6 and 7 compare the model products with buoys' data in dispersion graphs. In each figure, the data of the selected 21 buoys are illustrated by gray dots. Black dots show the data registered by the buoy 8°N 38°W. The panels on the left compare the salinity and the panels on the right compare the temperature data.

There is a large dispersion of surface salinity and temperature for the comparisons with OFES (Figure 5). The correlation was $r=0.87$ for salinity $r=0.84$ for temperature, with a confidence interval of 95%. The root mean squared error was 0.38 for salinity and 1.14 for temperature (Table 2). As previously verified, OFES fails to represent the salinity signal associated with the plumes' intrusion. Figure 6 presents the comparison to HYCOM reanalysis. Results reveal less dispersed data, yet without properly representing minimum salinity events. The correlation was $r=0.91$ for salinity, with RMSE of 0.30. Finally, Figure 7 compares in-situ data with the C-GLORS reanalysis. The product presented the smallest dispersion, with a correlation of $r=0.95$ for salinity and $r=0.98$ for temperature. The RMSE was 0.23 for salinity and 0.24 for temperature. C-GLORS presented the best comparisons with surface temperature and salinity observations.

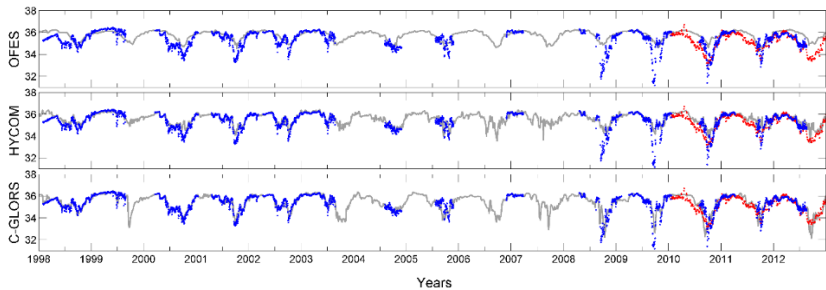


Figure 4. Time series of surface salinity from derived from observations and model products. Data from the PIRATA buoy of 8°N 38°W is indicated by blue dots. SMOS data for the same location are illustrated in red. Panels illustrate the different reanalysis products indicated by gray lines.

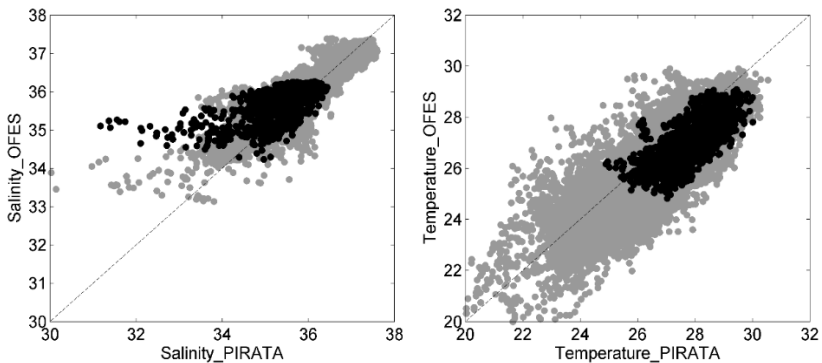


Figure 5. Dispersion diagrams of salinity in (psu) (left panel) and temperature in ($^{\circ}\text{C}$) (right panel) comparing PIRATA buoy observations to OFES model results. Gray dots represent the data of 21 buoys illustrated in Figure 1. Black dots represent the data of the buoy located at 8°N 38°W .

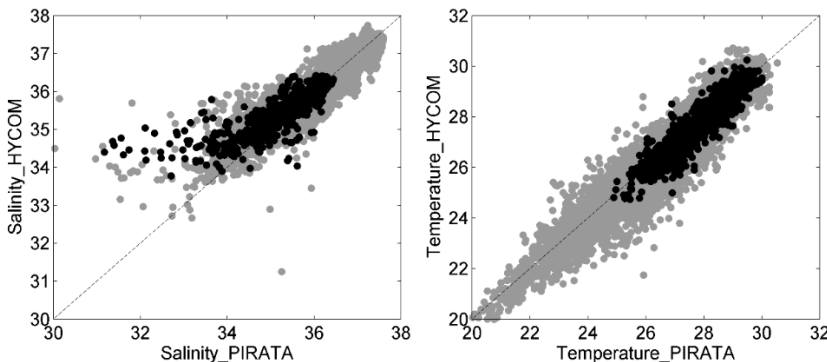


Figure 6. Similar to Figure 5 but for HYCOM model results.

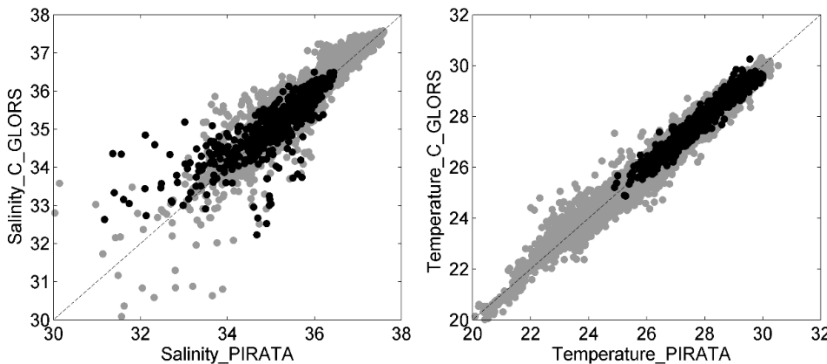


Figure 7. Similar to Figure 5 but for C-GLORS model results.

Table 2. Correlation and root mean squared error (in parentheses) for PIRATA salinity (S) and temperature (T) observations compared to model products. The location of the buoys is illustrated in Figure 1.

	Buoys 8°N 38°W		21 buoys	
	S	T	S	T
OFES	0.68 (0.67)	0.76 (1.10)	0.87 (0.38)	0.84 (1.14)
HYCOM	0.83 (0.49)	0.93 (0.39)	0.91 (0.30)	0.96 (0.47)
C-GLORS	0.86 (0.40)	0.97 (0.20)	0.95 (0.23)	0.98 (0.24)

3.3. Hydrographic profiles

This subsection compares CTD profiles from the hydrographical cruises with model data. Profiles were selected to intercept the core of the superficial low salinity layers present in the hidrographic observations. Figure 8 presents the results for the three different sections S1, S2 and S3 comparing the three model products. The left column displays salinity and the right column temperature profiles. The red line in each panel represents the observed profile (CTD). OFES is represented by a black line, HYCOM by green and C-GLORS by a blue line. The product that compares more favorably to in-situ data in the surface (0 to 200 m) is C-GLORS, and the worst is HYCOM with a difference up to 1 PSU in the surface. The salinity profile of section S1 illustrate a freshwater layer of 34.3 PSU up to 40 m depth. Below this superficial layer the profile indicates a halocline around 60 m.

Both HYCOM and C-GLORS presented a good performance for the temperature profiles. OFES has the largest differences for temperature in the surface and over deeper layers (>200 m). Below 200 m, both salinity and temperature profiles are generally well reproduced by HYCOM and C-GLORS. Table 3 shows the correlation results and the mean squared error of the salinity profiles presented in Figure 8.

C-GLORS stood out in all comparisons as the best model product for the Tropical Atlantic. After comparing its data with SMOS, PIRATA and hydrographic data, the conclusion was that C-GLORS reanalysis presents a rather satisfying performance for the study of freshwater dispersion processes. In the next section, the C-GLORS reanalysis product will be used to describe the different situations responsible for the formation of low salinity layers as recorded by the hydrographic observations.

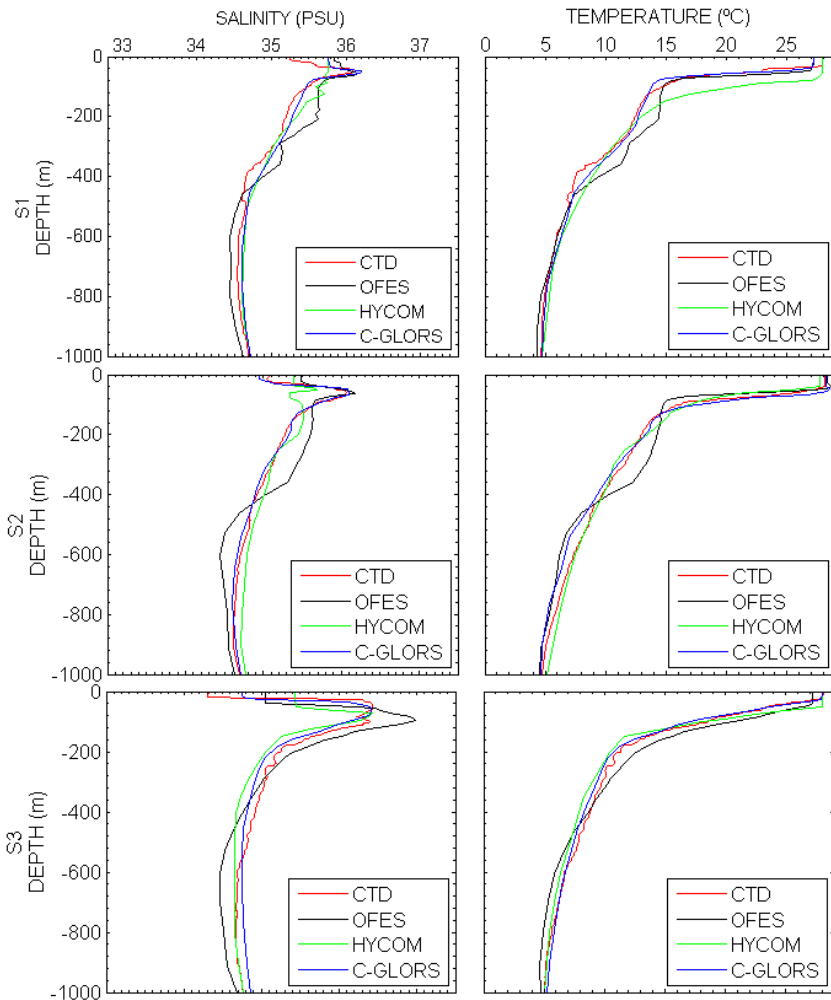


Figure 8. Salinity (left panels) and temperature (right panels) profiles derived from hydrographic transects S1, S2 and S3, comparing hydrographic data (CTD, red line) to model data from OFES (black), HYCOM (green) and C-GLORS (blue). The positions of the profiles will be show below in the figure 9, 11 e 14 identified with a square magenta.

Table 3. Correlation and mean squared error (in parentheses) between the reanalysis products and the vertical profiles of salinity. The data refer to the stations selected from the transects S1, S2 and S3, illustrated in Figure 8.

	S1	S2	S3
OFES	0.91 (0.36)	0.96 (0.19)	0.93 (0.20)
HYCOM	0.86 (0.27)	0.96 (0.13)	0.92 (0.15)
C-GLORS	0.96 (0.14)	0.98 (0.10)	0.99 (0.04)

3.4. Hydrographic transects and low salinity band formation

In this subsection, C-GLORS data is used to explore the background oceanographic setting during the sampling of the hydrographic sections S1, S2 and S3 (Figure 1 and Table 1). Both large-scale ocean currents and regional precipitation can play a fundamental role in the intrusion of coastal plumes and the formation of low salinity surface layers in the Tropical Atlantic.

3.4.1. Transect S1 at 44°W

Figure 9 (left panel) presents the hydrographic section S1 at the longitude 44°W derived from the Meteor cruise M151 of November 2000 and compares its data to the results of C-GLORS reanalysis (right panel). A deep halocline is observed around 150 m with a salinity limit close to 35.5 PSU as well as a shallower halocline at 50 m, delimiting a low salinity surface layer between 5° and 11°N.

The low salinity surface structure illustrate two cores of approximately 34.5 PSU separated by one degree of latitude, surrounded by tropical ambient waters (> 36 PSU). The C-GLORS data demonstrate the same structures in the hydrographic section.

The evolution of surface salinity fields and precipitation enable the exploration of the formation mechanism of this low salinity surface layer. Figure 10 presents six panels: the first illustrates the accumulated precipitation in June 2000 (panel A). The following panels (B to F) show the evolution of the surface salinity between June 28th and November 13th of 2000. Virtual Lagrangian drifters are also indicated. Those launched instantaneously into the precipitation core located at 8°N and 35°W in June 2000 are illustrated by black dots. Drifters launched continuously in the mouth of the Amazon estuary are illustrated by white dots.

Particles released in the mouth of the Amazon follow the NBC retroflection and travel around 8°N through the NECC. Yet, the particles liberated into the precipitation core follow two main paths. Some particles migrate to the east with the NECC and others migrate to the west through the nSEC, providing the mixing of relatively fresh waters from the Amazon plume with waters from precipitation. Wind-driven currents, however, participate redistributing the less saline waters zonally.

The most common view of the hydrologic cycle establishes estuarine plumes as the final destination of waters derived from continental precipitation. The results showed here, however, refer to an evidence that large-scale plumes can also be the destination of waters originated from ocean precipitation. These waters can refuel the coastal plumes maintaining their saline anomaly in the far field.

The panel F of Figure 10 denotes the situation of convergence and mixture of fresh waters over the hydrographic section S1 collected in November 2000. Such results suggest the intrusion of the Amazon plumes in its far field has significant contributions of waters derived from ITCZ cores, which deform in zonal bands due to the shear of wind-driven currents.

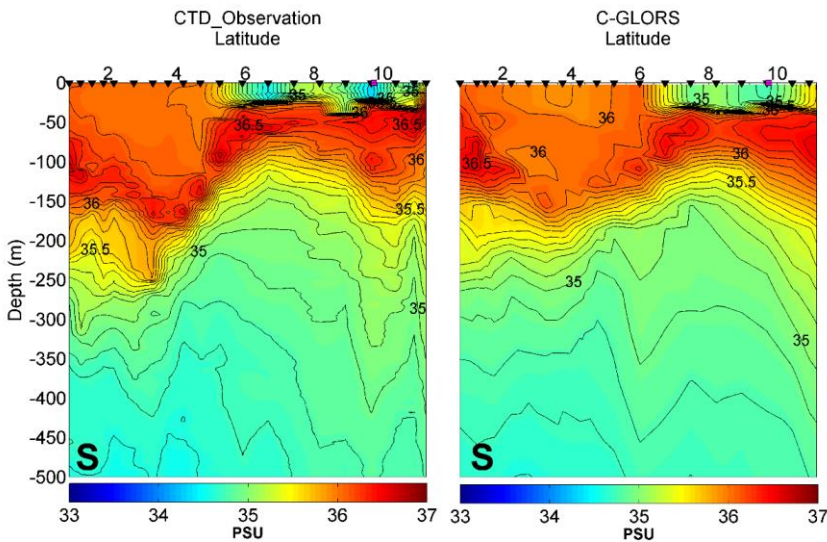


Figure 9. Vertical salinity transect S1 at 44° W from the Meteor cruise M151 of November 2000, compared to C-GLORS model results for the same period. The salinity is indicated by colors with contour interval of 0.1 psu. Black triangles show the position of the CTD profiles and a square shows the position of the profile illustrated in Figure 8.

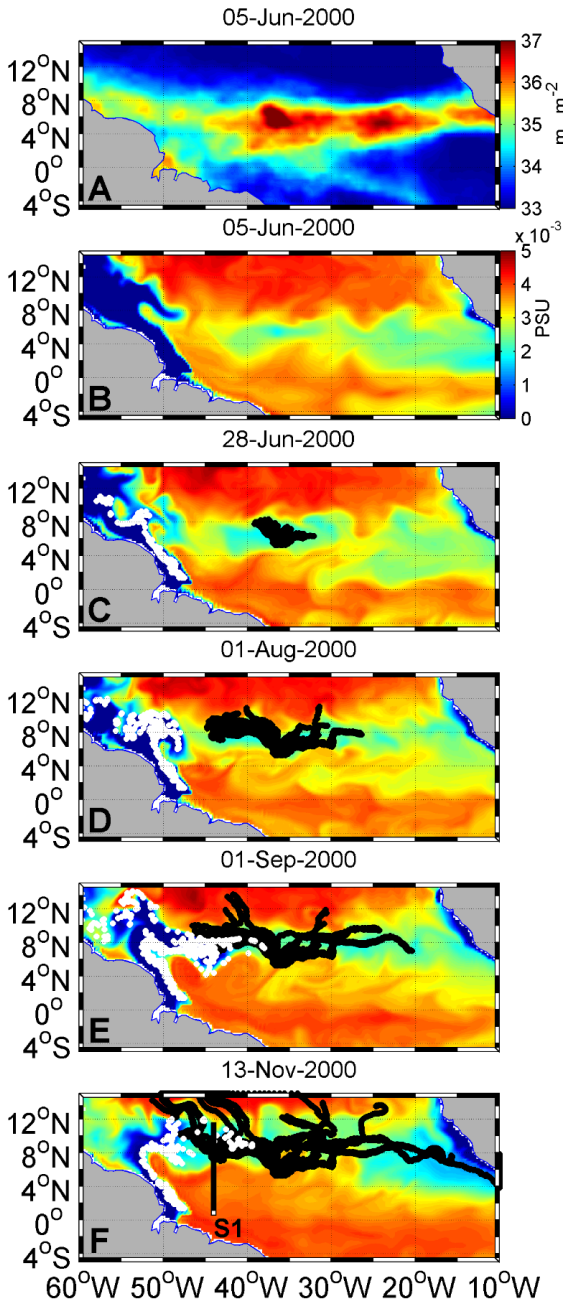


Figure 10. Evolution of the oceanographic conditions before the sampling of transect S1 during the Meteor cruise M151 of November 2000 (Table 1). Panel A describes the precipitation field of June 5th, 2000. The next panels (B to F) illustrate the evolution of the salinity field from June 5th to November 13th, 2000. Black dots illustrate the trajectory of particles instantaneously launched into the precipitation core located at 8°N 35°W. The trajectory of the particles illustrates the mixing of Amazon plume with the waters derived from oceanic precipitation. The position of transect S1 is indicated.

3.4.2. *Transect S2 at 35°W*

Figure 11 presents the salinity hydrographic section for the transect S2 at 35°W of May 2002 along with the C-GLORS dataset. A halocline between 100 and 150 m separates tropical waters in the surface (TW) from South Atlantic Central Water at greater depths (SACW) (Stramma and England, 1999). Two subsurface cores of high salinity are observed at 0° and 4°S respectively. The first is associated with the Equatorial Undercurrent (EUC); the second is associated with the North Brazil Undercurrent (NBUC) (Schott et al., 2005).

The layer with the lowest salinity detected in the surface during the cruise is also present in the reanalysis product. Anomalies are on the order of 1 to 2 PSU in the surface compared to tropical waters up to 37 PSU. The surface layer has two cores, one located at 3°S and the other at 3°N.

Figure 12 illustrates the streamlines as well as the average salinity field for May of 2002. The fresh waters detected in this situation cannot be associated with the Amazon plume which was at the beginning of its intrusion. The same analysis is valid for the freshwater derived from the African coast which is around 20°W to the west of the Gulf of Guinea. The analysis of the salinity and currents field suggest that the low salinity layer observed during the cruise was associated with the precipitation.

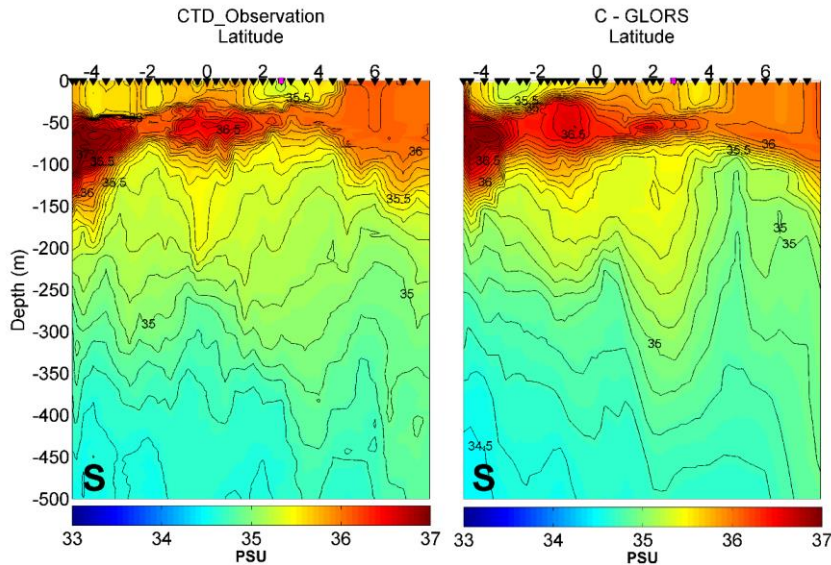


Figure 11. Vertical salinity transect S2 at 35°W during the Meteor cruise M53, compared to the results of the reanalysis C-GLORS for May 2002. The salinity is indicated by colors with contour interval of 0.1 psu. Black triangles show the position of the CTD profiles and a square shows the position of the profile illustrated in Figure 8.

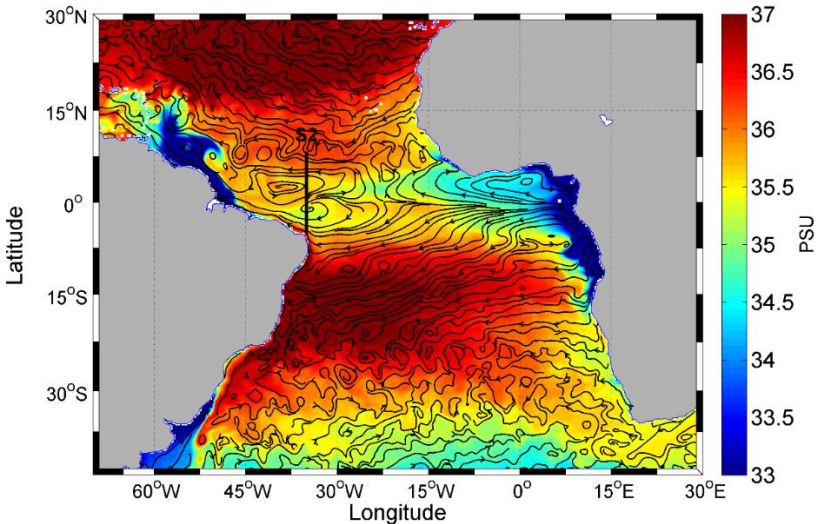


Figure 12. Surface salinity and streamlines from C-GLORS for May 2002, sampling period of the transect S2 at 35°W as part of the cruise Meteor M53 (Table 1). The position of the section is indicated by a black line. It is noted that in this period, the Amazon plume is starting its retro-reflection along with the NBC. On the African coast, the waters of the Gulf of Guinea are still confined to 15°W .

3.4.3. Transect S3 at 28°W

The hydrographic section S3 at 28°W of June 2006 conducted by the Meteor cruise M68 is illustrated in Figure 13 (left panel). The features of deeper and surface layers are well represented by the model. The halocline at 100 m separates tropical waters in the surface from deeper central waters. A wide structure stands out in the hydrographic data. It refers to a “V” shape low salinity lens between 0° to 10°N . This layer has 70 m depth and salinity anomalies on the order of 1 to 2 PSU compared to the ambient waters.

Streamlines overlaid on surface salinity fields for the period of the M68 cruise are illustrated in Figure 14. The position of the transect S3

is indicated by a black line, demonstrating how the cruise intercepted the core of the freshwater intrusion from the African coast. As the streamlines illustrate, Gulf of Guinea's waters are advected by the nSEC at 2°N to 30°W , then are deflected to the north, merging with the Amazon waters along the NECC.

Figure 15 illustrates the evolution of this episode, displaying the salinity and the streamlines fields two months later, in August 2006. This figure illustrates the wide extension of the Amazon plume advected by the NECC and the formation of a low salinity zonal band due its encounter with lower salinity waters derived from the Gulf of Guinea. The freshwater transport from the African coast is promoted by the nSEC.

Part of the freshwater is detained inside the equatorial gyre, recirculating through the nSEC current (west direction) and NECC (east direction). The lower panel of Figure 15 illustrates the vertical section through this low salinity zonal band at 7°S . The surface layer is 40 m depth and extends for more than 4200 km from the South American to the African coast.

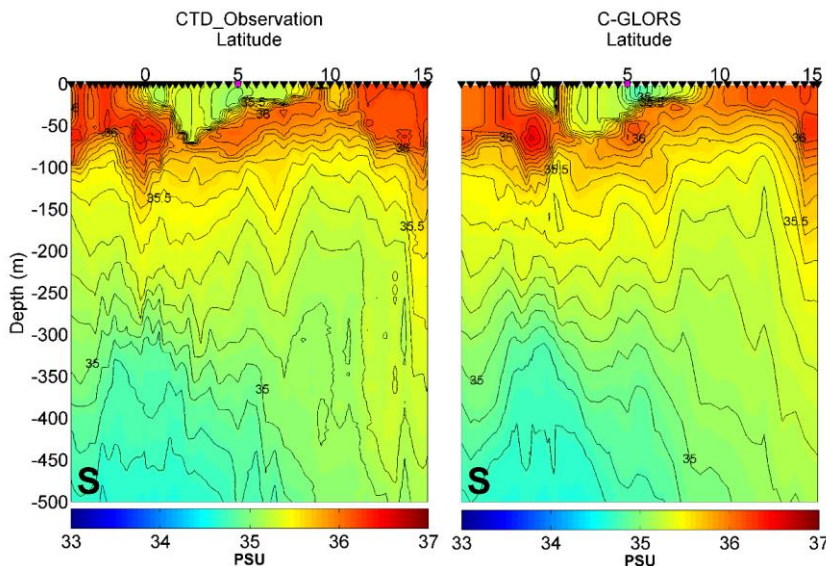


Figure 13. Vertical salinity transect S3 at 28°W during the Meteor cruise M68, compared to the results of the reanalysis C-GLORS for June 2006. The salinity is indicated by colors with contour interval of 0.1 psu. Black

triangles show the position of the CTD profiles and a square shows the position of the profile illustrated in Figure 8.

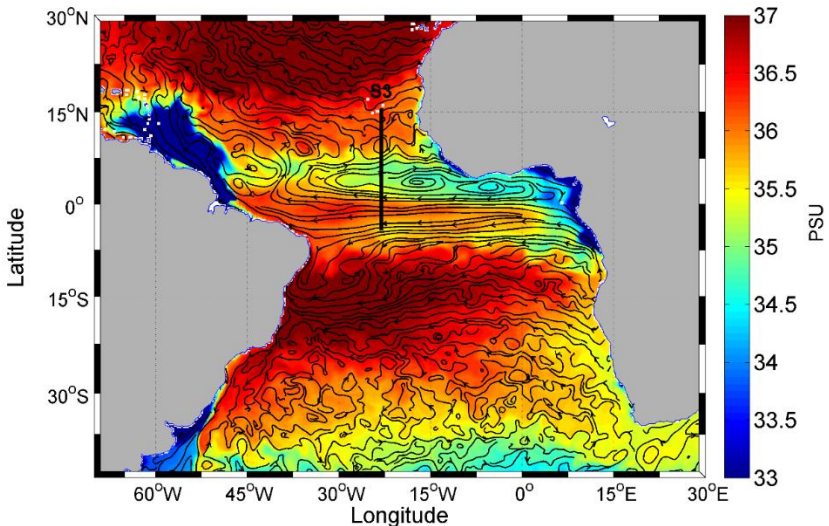


Figure 14. Surface salinity field and streamlines derived from C-GLORS for June 2006, sampling period of the transect S3 at 28°W during the cruise Meteor M68 (Table 1). The position of the section is indicated by a black line. It is noted that in this period, the Amazon plume is starting its intrusion along with the NECC. In this situation, the equatorial gyre formed by the nSEC is quite developed, transporting freshwaters from the Gulf of Guinea to the longitude of 35°W.

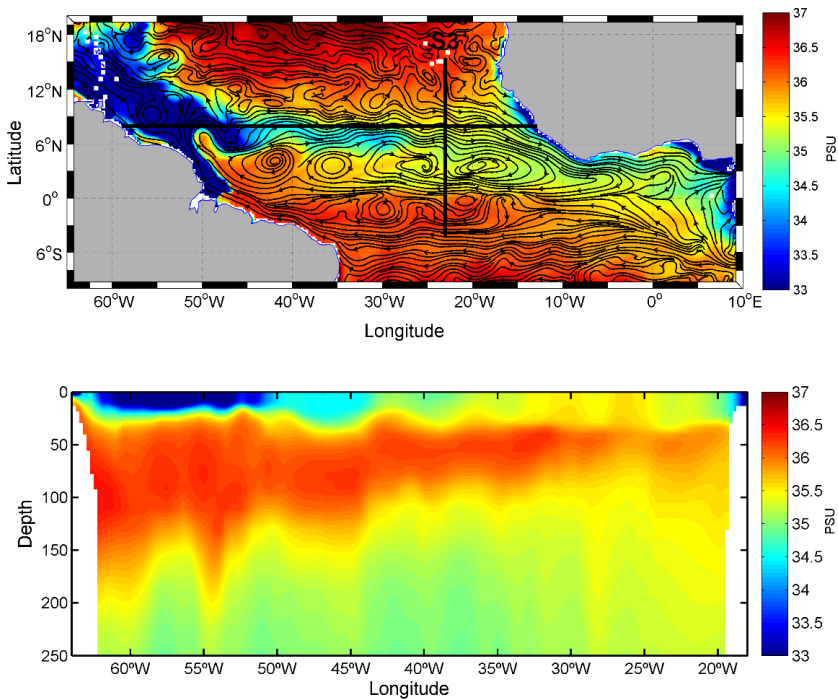


Figure 15. a) Surface salinity fields and streamlines derived from C-GLORS for August 2006. The figure illustrates the intrusion of the Amazon plume along the NECC, interacting with waters coming from the Gulf of Guinea, transported by nSEC. The mixing of these different freshwater sources leads to the formation of a continuous low salinity zonal band between 3°N and 8°N. b) Vertical transect between 18° and 65°W illustrating the structure of the low salinity zonal band. As it is illustrated, the surface layer has salinity between 33 and 34.5 and depth of approximately 40 meters.

3.5. Seasonal variability

The previous analysis suggests that the formation of low salinity zonal bands has significant contributions from the Amazon River plume advected by the NECC and from Gulf of Guinea river and precipitation freshwaters advected by the nSEC. In order to explore the variability of these intrusions, we monitored the position of the 34.5 isoline around the latitudes of 8°N and 4°N, presenting the results in Figure 16. Here the abscissa represents the zonal position of these freshwater intrusions. Black dots describe the climatological variability of intrusions under influence of Amazon River plume at 8°N. Red squares illustrate the average displacement of freshwaters intrusions from the African coast at 4°N.

We can observe that the plumes are generally close to the coast during the first half of the year (January to April). Over the months, the low salinity waters are transported offshore, reaching maximum intrusions on the second half of the year. The climatological maximum occurs in September for the Amazon plume and between August and October for the Gulf of Guinea freshwaters. These migrations are dominantly controlled by zonal currents. The intrusion of the Amazon plume has shorter duration when compared to the intrusion of the waters coming from the contribution of rivers and precipitation over the Gulf of Guinea.

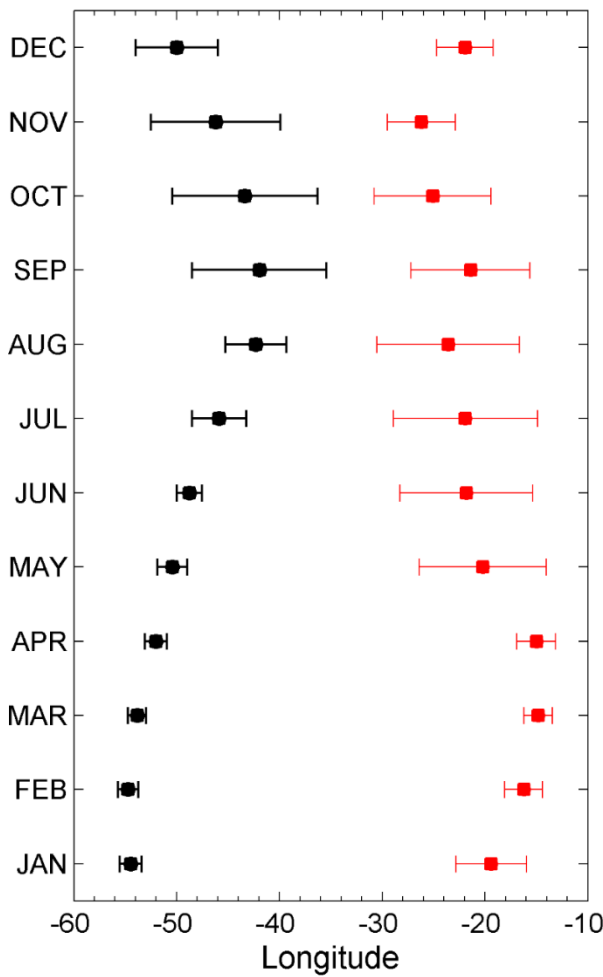


Figure 16. Climatology of the low salinity intrusions on the Tropical Atlantic. Black dots indicate the average position of the 34.5 PSU isohaline along the latitude of 8°N. Red dots indicate the isoline of 34.5 PSU position for the latitude of 4°N (red). Bars indicate the standard deviation. Data used refers to the surface salinity fields of C-GLORS between 1993 and 2014.

3.6. Interannual variability

Figure 17 illustrates the surface salinity temporal evolution through a Hovmöller diagram at 8°N, illustrating the year-to-year variability of low salinity band formation between 1993 and 2014 (central panel). The isolines of 34.5 and 35 PSU are indicated, as well as the position and period covered by the hydrographical cruises (black squares). The same figure presents the time series of river discharges (left panel) and integrated precipitation (right panel).

The river discharges of the Amazon and Tocantins river (red) and time series of the Orinoco (blue) and Congo (black) rivers come from Dai et al. (2009). The Amazon river has a strong seasonal signal, with a maximum of discharge in the first semester, reaching close to 250000 m³ s⁻¹. The Orinoco and Congo rivers have maximums of 68.000 e 82.000 m³ s⁻¹ in July and November respectively. The correlation of the Amazon river's discharge with salinity at 8°N 35°W is relatively low, r=0.56, with a confidence interval of 95%.

The integrated precipitation in the tropical region between 15°N and 15°S is significant. Its contribution is equal to an average discharge of 315.000 m³ s⁻¹, thus comparable the sum of the discharges of the Amazon, Orinoco and Congo rivers. Different from the river discharge, the integrated precipitation does not present any dominant seasonal signal and is apparently uncorrelated (r=0.23) to the salinity signal at 8°N 35°W.

The time series of integrated precipitation for the region close the Amazon mouth (A2) and the Gulf of Guinea region (A3) are illustrated as black and red lines respectively (Figure 17). The contribution of precipitation on these regions is comparable to the discharge of the Orinoco and Congo rivers, although they do not present any clear correlation with low band formation or the salinity signal at 35°W.

The analysis of the Hovmöller diagram made for the latitude 8°N corroborates the climatological results described in the previous section. Low salinity intrusions happen preferentially during the second semester after the seasonal peak of Amazon discharge, with a signal that

propagates to the east, from the South American coast at 60°W . The westward intrusion of freshwater from the African coast at 10°W is also apparently in synch with Congo discharge which has its maximum on November.

The salinity field illustrates that in the years 1997, 2000, 2006, 2008, 2011 and 2012, these freshwater intrusions were so significant that they formed a continuous low salinity zonal band. The weak correlation with the river discharge and the integrated precipitation suggests that the formation of the low salinity band might be attributed to the variability of the wind-driven circulation.

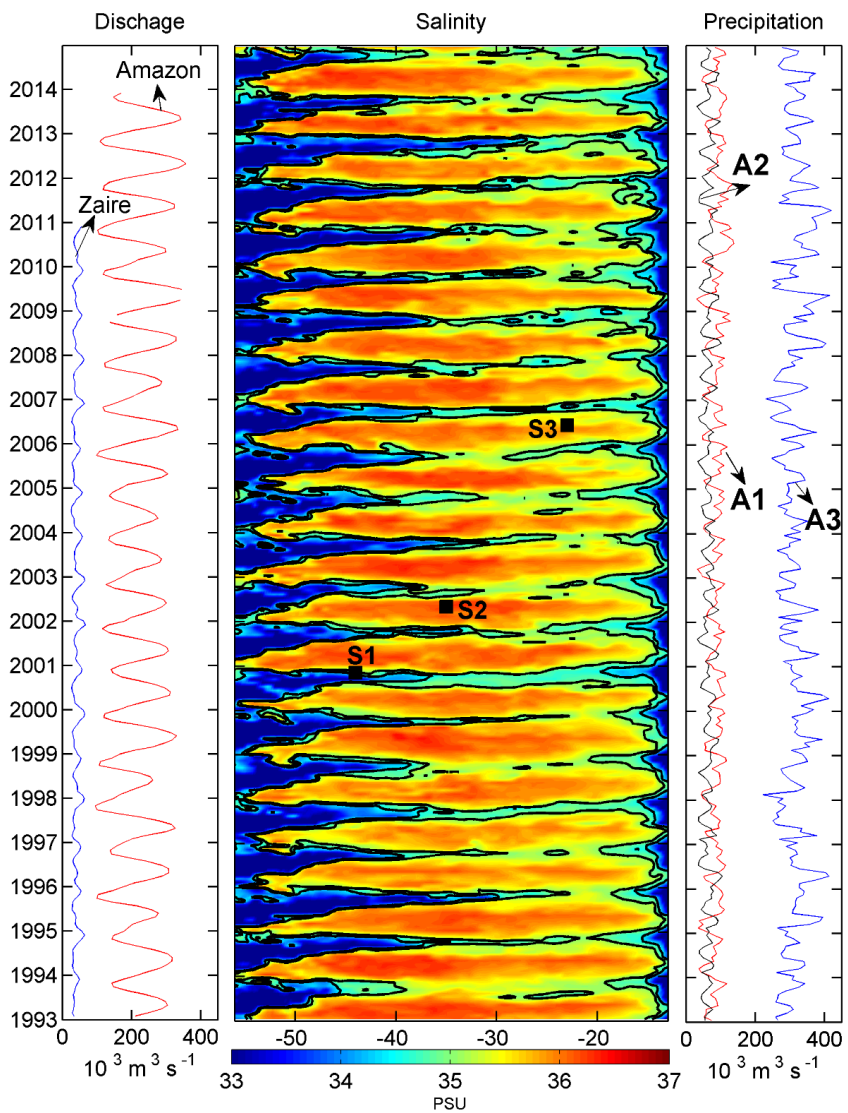


Figure 17. Hovmöller diagram indicating the year-to-year variability on the formation of continuous low salinity zonal bands in the Tropical Atlantic at 8°N (central panel). The left panel indicates temporal series of the river discharges of the Amazon+Tocantins, Orinoco and Congo rivers

(Dai et al., 2009). The panel on the right illustrates the integrated precipitation series for the regions indicated in Figure 1b: the region of the Gulf of Guinea (A1); the region of the Amazon plume (A2) and the tropical region between 15°N and 15°S (A3). The formation of salinity zonal band was significant for 1997, 2000, 2006, 2008, 2011 and 2012.

4. SUMMARY AND CONCLUSIONS

This article explored the dynamics of low latitude plumes derived from large river discharges of the Tropical Atlantic, exploring the role precipitation and of wind-driven large-scale currents in the intrusion and maintenance of these structures.

Three model products (OFES, HYCOM and C-GLORS) were compared with satellite data from SMOS, historical hydrographic data and PIRATA buoys in order to select the best product. Surface salinity fields were well described by the reanalysis C-GLORS when compared to the satellite product. The correlations of PIRATA time series against OFES, HYCOM and C-GLORS were 0.87, 0.91 and 0.95 with a mean squared error (RMSE) of 0.38, 0.30 and 0.23 PSU respectively.

Although C-GLORS has less spatial resolution, its performance was more satisfying than the other products. Tseng et al. (2016) shows that the current climate models do not explicitly resolve mixing processes and that better parameterizations are necessary. Despite the fact that the products HYCOM and C-GLORS have advanced systems of data assimilation, C-GLORS was the only model capable to satisfactorily reproduce the salinity fields. This was partially linked to the prescription of the river discharge employed by C-GLORS.

The analysis of the historical hydrographic sections, combined with the C-GLORS product illustrated the process of dispersion of the Amazon plume and the low salinity waters of the Gulf of Guinea. During the first semester of the year, the Amazon and Orinoco waters follow the North Brazil Current (NBC) to the Caribbean. During the second semester - the Amazon plume is captured in the NBC retroflection, which flows to the east, through the North Equatorial Countercurrent (NECC) at 8°N.

During its intrusion, the plume receives the contribution of precipitation from the ITCZ, which converge with the equatorial currents mixing with Amazon waters.

On the east side, the Gulf of Guinea gyre accumulates low salinity waters derived from large African rivers such as the Congo, Niger and Sanaga as well as freshwaters from ocean precipitation. At the beginning of the year the Gulf of Guinea plume remains close to the African coast. In July, it starts its intrusion to the west, flowing with the northern branch of the South Equatorial Current (nSEC).

In certain occasions, the extension of the Amazon plume to the west and the extension of the Gulf of Guinea waters to the east leads to their convergence forming of a continuous low salinity zonal band. The reanalysis suggests that the zonal band formation has year-to-year variability, presumably associated with wind-driven currents. Foster et al. (2009) showed that the same nitrogen fixed with communities associated with the Amazon river plume was also found in the fresh water of the Gulf of Guinea. This fact suggests a biological connectivity between the two regions.

To conclude, the intrusion of freshwater has a much bigger impact than what current global models reproduce (Sun et al., 2017). Coles et al. (2013) suggest that freshwater plumes strengthen the vertical stratification, reducing the mixed layer depth, also modifying currents and the ocean-atmosphere interactions. As the area of this low salinity zonal band formation is prone to the passage of hurricanes, it is necessary to implement the dynamics of this band for more realistic atmospheric forecasts.

5. ACKNOWLEDGMENTS

FR thanks CAPES (Sea Science Project II-Edital 43/2013) for the grant along with PPGOceano/UFSC. FMP thanks CNPq (process 486381/2013-7, 406801/2013-4, 311930/2016-6). We thank Dr. Denny Kirwan for the routine of Lagrangian trajectories and Dr. Peter Brandt for his early suggestion of comparisons to the TACE historical data. Dr. Storto provided an earlier version of C-GLORS datset.

6. REFERENCES

- Balaguru, K., P. Chang, R. Saravanan, L. R. Leung, Z. Xu, M. Li, and J.-S. Hsieh, 2012: Ocean barrier layers' effect on tropical cyclone intensification. *pnas*, 109 (36), 14343?14347, doi:10.1073/pnas.1201364109.
- Berger, H., A. M. Treguier, N. Perenne, and C. Talandier, 2014: Dynamical contribution to sea surface salinity variations in the eastern Gulf of Guinea based on numerical modelling. *Climate dynamics*, 43 (11), 3105-3122.
- Bourlès, B., et al., 2008: The pirata program: history, accomplishments, and future directions. *Bulletin of the American Meteorological Society*, 89 (8), 1111-1125.
- Castelão, G. P. and W. E. Johns, 2011: Sea surface structure of north Brazil Current rings derived from shipboard and moored acoustic doppler current profiler observations. *J. Geophys. Res.*, 116 (C1), doi:10.1029/2010JC006575, URL <http://dx.doi.org/10.1029/2010JC006575>, c01010.
- Cavalcanti, I. F. A., N. J. Ferreira, M. G. A. J. Silva, and M. A. F. Silva Dias, 2009: *Tempo e clima no Brasil*. O?cina de Textos, São Paulo, 463 pp.
- Chao, Y., J. D. Farrara, G. Schumann, K. M. Andreadis, and D. Moller, 2015: Sea surface salinity variability in response to the Congo River discharge. *Continental Shelf Research*, 99, 35-45.
- Coles, V. J., M. T. Brooks, J. Hopkins, M. R. Stukel, P. L. Yager, and R. R. Hood, 2013: The pathways and properties of the Amazon River plume in the tropical north atlantic ocean. *Journal of Geophysical Research: Oceans*, 118 (12), 6894-6913.
- Dai, A., T. Qian, K. E. Trenberth, and J. D. Milliman, 2009: Changes in continental freshwater discharge from 1948-2004. *J. Clim.*, 22, 2773-2791.

- Dai, A. and K. E. Trenberth, 2002: Estimates of freshwater discharge from continents: Latitudinal and seasonal variations. *J. Hydrol.*, 3, 660-687.
- Denamiel, C., W. P. Budgell, and R. Toumi, 2013: The congo river plume: Impact of the forcing on the far-field and near-field dynamics. *Journal of Geophysical Research: Oceans*, 118 (2), 964-989.
- Dobricic, S. and N. Pinardi, 2008: An oceanographic three-dimensional variational data assimilation scheme. *Ocean modelling*, 22 (3), 89-105.
- Eisma, D. and A. Van Bennekom, 1978: The zaire river and estuary and the Zaire outflow in the atlantic ocean. *Netherlands Journal of Sea Research*, 12 (3-4), 255-272.
- Ffeld, A., 2007: Amazon and Orinoco River plumes and NBC rings: bystanders or participants in hurricane events? *Journal of climate*, 20 (2), 316-333.
- Fong, D. A. and W. R. Geyer, 2001: Response of a river plume during an upwelling favorable wind event. *J. Geophys. Res.*, 106 (C1), 1067-1084.
- Fong, D. A. and W. R. Geyer, 2002: The alongshore transport of freshwater in a surface-trapped river plume. *J. Phys. Oceanogr.*, 32, 957-972.
- Foster, R. A., A. Subramaniam, and J. P. Zehr, 2009: Distribution and activity of diazotrophs in the eastern equatorial Atlantic. *Environmental microbiology*, 11 (4), 741-750.
- Garvine, R. W., 1995: A dynamical system for classifying buoyant coastal discharges. *Cont. Shelf Res.*, 13, 1585-1596.
- Garvine, R. W., 1999: Penetration of buoyant coastal discharge onto the continental shelf: A numerical model experiment. *J. Phys. Oceanogr.*, 29, 1892-1909.

- Geyer, W. R., R. C. Beardsley, S. J. Lentz, J. Candela, R. Limeburner, W. E. Johns, B. M. Castro, and I. D. Soares, 1996: Physical oceanography of the Amazon shelf. *Cont. Shelf Res.*, 16, 575-616.
- Hovius, N., 1998: Controls on sediment supply by large rivers. Relative role of eustasy, climate and tectonism in continental rocks, S. K. M. and M. P. J., Eds., Society for Sedimentary Geology, SEPM, Vol. 59, 4-15, tulsa, OK.
- Ingleby, B. and M. Huddleston, 2007: Quality control of ocean temperature and salinity profiles-historical and real-time data. *Journal of Marine Systems*, 65 (1), 158-175.
- Kalnay, E., et al., 1996: The NCEP/NCAR 40-year reanalysis project. *Bull. Amer. Meteor. Soc.*, 77, 437-471.
- Kerr, Y. H., et al., 2010: The SMOS mission: New tool for monitoring key elements of the global water cycle. *Proceedings of the IEEE*, 98 (5), 666-687.
- Korosov, A., F. Counillon, and J. A. Johannessen, 2015: Monitoring the spreading of the amazon freshwater plume by MODIS, SMOS, AQUARIUS, and topaz. *Journal of Geophysical Research: Oceans*, 120 (1), 268-283.
- Large, W. G. and S. G. Yeager, 2004: Diurnal to decadal global forcing for ocean and sea-ice models: the data sets and flux climatologies. National Center for Atmospheric Research Boulder.
- Lentz, S. J., 2004: The response of buoyant coastal plumes to upwelling favorable winds. *J. Phys. Oceanogr.*, 34, 2458-2469.
- Lentz, S. J. and J. Largier, 2006: The influence of wind forcing on the Chesapeake Bay buoyant coastal current. *J. Phys. Oceanogr.*, 36, 1305-1316.
- Lentz, S. J. and R. Limeburner, 1995: The Amazon River plume during AMASSEDS: Spatial characteristics and salinity variability. *Journal of Geophysical Research: Oceans*, 100 (C2), 2355-2375.

- Madec, G., P. Delecluse, M. Imbard, and C. Levy, 1998: Opa 8 ocean general circulation model - reference manual. Tech. rep., LODYC/IPSL Note 11.
- Masumoto, Y., et al., 2004: A fifty-year eddy-resolving simulation of the world ocean: Preliminary outcomes of ofes (ogcm for the earth simulator). *J. Earth Simulator*, 1, 35-56.
- Muller-Karger, F. E., C. R. McClain, and P. L. Richardson, 1988: The dispersal of the amazon's water. *Nature*, 333 (6168), 56-59.
- Pacanovsky, R. and S. Griffies, 1999: The mom 3 manual. geophysic fluid dynamics laboratory. NOAA, Princeton; USA, 680, 680.
- Pailler, K., B. Bourlès, and Y. Gouriou, 1999: The barrier layer in the western tropical atlantic ocean. *Geophysical Research Letters*, 26 (14), 2069-2072.
- Palma, E. D. and R. P. Matano, 2017: A an idealized study of near equatorial river plumes. *J. Geophys. Res.*, 122, doi:10.1002/2016JC012554.
- Pimenta, F. M., J. A. D. Kirwan, and P. Huq, 2011: On the transport of buoyant coastal plumes. *J. Phys. Oceanogr.*, 41 (1), 620-640.
- Reul, N., Y. Quilfen, B. Chapron, S. Fournier, V. Kudryavtsev, and R. Sabia, 2014: Multisensor observations of the amazon-orinoco river plume interactions with hurricanes. *Journal of Geophysical Research: Oceans*, 119 (12), 8271-8295.
- Rosati, A. and K. Miyakoda, 1988: A general circulation model for upper ocean simulation. *Journal of Physical Oceanography*, 18 (11), 1601-1626.
- Schiller, R. V. and V. H. Kourafalou, 2010: Modeling river plume dynamics with the HYbrid Coordinate Ocean Model. *Ocean Modelling*, 33 (1), 101-117, doi:<https://doi.org/10.1016/j.ocemod.2009.12.005>.
- Schott, F. A., M. Dengler, R. Zantopp, L. Stramma, J. Fischer, and P. Brandt, 2005: The shallow and deep western boundary circulation of

- the south atlantic at 5-11 s. *Journal of Physical Oceanography*, 35 (11), 2031-2053.
- Storto, A., S. Dobricic, S. Masina, and P. Di Pietro, 2011: Assimilating along-track altimetric observations through local hydrostatic adjustment in a global ocean variational assimilation system. *Monthly Weather Review*, 139 (3), 738-754.
- Storto, A., S. Masina, and A. Navarra, 2016: Evaluation of the cmcc eddy-permitting global ocean physical reanalysis system (c-glors, 1982-2012) and its assimilation components. *Quarterly Journal of the Royal Meteorological Society*, 142 (695), 738-758.
- Storto, A., I. Russo, and S. Masina, 2012: Interannual response of global ocean hindcasts to a satellite-based correction of precipitation fluxes. *Ocean Sci. Discuss.* 9, 611-648., doi:<https://doi.org/10.5194/osd-9-611-2012>.
- Stramma, L. and M. England, 1999: On the water masses and mean circulation of the South Atlantic ocean. *J. Geophys. Res.*, 104 (C9), 20863-20883.
- Sun, Q., M. M. Whitney, F. O. Bryan, and Y.-h. Tseng, 2017: A box model for representing estuarine physical processes in earth system models. *Ocean Modelling*, 112, 139-153.
- Tseng, Y.-h., F. O. Bryan, and M. M. Whitney, 2016: Impacts of the representation of riverine freshwater input in the community earth system model. *Ocean Modelling*, 105, 71-86.
- Wallcraft, A., E. Metzger, and S. Carroll, 2009: Software design description for the hybrid coordinate ocean model (hycom), version 2.2. Tech. rep., NAVAL RESEARCH LAB STENNIS SPACE CENTER MS OCEANOGRAPHY DIV.
- Whitney, M. M. and R. W. Garvine, 2005: Wind influence on a coastal buoyant outflow. *J. Geophys. Res.*, 110 (C03014), 1437-1483, doi: 10.1029/2003JC002261.
- Yankovsky, A. E. and D. C. Chapman, 1997: A simple theory for the fate of buoyant coastal discharges. *J. Phys. Oceanogr.*, 27, 1386-1401.

5. CONCLUSÕES E CONSIDERAÇÕES FINAIS

Esta dissertação explorou a dinâmica de plumas de baixa latitude derivadas de grandes descargas fluviais do Atlântico Tropical, explorando o papel da precipitação e das correntes de larga escala dirigidas pelo vento na intrusão e manutenção destas estruturas. Três produtos de modelagem oceânica (OFES, HYCOM e C-GLORS) foram comparados com dados satelitários SMOS, dados hidrográficos históricos e dados de boias PIRATA, para seleção de um produto que melhor representasse o Atlântico Tropical. Campos de salinidade superficial foram bem descritos pela reanálise C-GLORS em comparação ao produto satelitário SMOS. Correlações das séries temporais de salinidade PIRATA contra os produtos OFES, HYCOM e C-GLORS foram 0.87, 0.91 e 0.95 com um erro quadrático médio (RMSE) de 0.38, 0.30 e 0.23 psu respectivamente.

Embora o C-GLORS possua menor resolução espacial que outros produtos, seu desempenho foi mais satisfatório. Tseng et al. (2016) destaca que os modelos climáticos atuais não resolvem explicitamente os processos de mistura costeiro-estuarina, sendo necessário parametrizações. Embora os produtos HYCOM e C-GLORS possuem avançados sistemas de assimilação de dados, somente o C-GLORS foi capaz de modelar satisfatoriamente o campo superficial termohalino no Atlântico Tropical. Este fato está provavelmente associado a prescrição da descarga fluvial realizada pelo C-GLORS.

A análise de seções hidrográficas históricas, combinada ao produto C-GLORS ilustrou o processo de dispersão da pluma do Amazonas e das águas de baixa salinidade do Golfo da Guiné. No primeiro semestre do ano, as águas do Amazonas e Orinoco seguem a Corrente Norte do Brasil (NBC) em direção ao Caribe. No segundo semestre, a partir de agosto, a pluma do Amazonas é capturada na retroflexão da NBC, posteriormente fluindo para leste através da Contracorrente Norte Equatorial (NECC) a 8° N. Durante sua intrusão, a pluma sofre a contribuição de águas derivadas da precipitação da ITCZ, que convergem ao longo das correntes equatoriais, misturando-se com as águas do Amazonas.

No lado leste, o interior do Giro da Guiné concentra águas de baixa salinidade oriundas dos grandes rios Africanos, como Congo, Niger

e Sanaga, além de águas frescas derivadas da precipitação oceânica. Verificamos um padrão sazonal de migração das águas do Giro da Guiné. No início do ano está pluma encontra-se retraída próximo à costa da África. A partir de julho ela inicia sua intrusão à oeste, fluindo através do ramo norte da Corrente Sul Equatorial (nSEC).

Em certas ocasiões, a extensão da pluma do Amazonas, para oeste, e das águas do Golfo da Guiné, para leste, leva a convergência de águas frescas, com a formação de uma banda zonal contínua de baixa salinidade. A reanálise sugere que o fenômeno de formação da banda possui variabilidade interanual, presumivelmente associado a variações das correntes oceânicas. Foster et al. (2009) mostrou que o mesmo nitrogênio fixado com comunidades associadas a Pluma do Rio Amazonas, também foram encontradas junto à água fresca encontrada no Golfo da Guiné, sugerindo conectividade biológica entre as regiões.

Finalizando, a intrusão de água fresca tem um impacto maior do que é atualmente reproduzido por modelos climáticos globais (Sun et al., 2017). Coles et al. (2013) destaca que plumas de água fresca introduzem estratificação que pode reduzir a camada de mistura, modificar correntes, e influenciar a interação oceano-atmosfera. Visto que a área de formação desta banda zonal de baixa salinidade é uma região de origem e passagem de furacões, há a necessidade de implementar a dinâmica desta banda para previsões atmosféricas mais realísticas.

6. REFERÊNCIAS

- Berger, H., Treguier, A. M., Perenne, N. and Talandier, C. (2014), Dynamical contribution to sea surface salinity variations in the eastern gulf of guinea based on numerical modelling, *Climate dynamics* 43(11), 3105-3122.
- Bourlès, B., Lumpkin, R., McPhaden, M. J., Hernandez, F., Nobre, P., Campos, E., Yu, L., Planton, S., Busalacchi, A., Moura, A. D. et al. (2008), The PIRATA program: history, accomplishments, and future directions, *Bulletin of the American Meteorological Society* 89(8), 1111-1125.

- Cavalcanti, I. F. A., Ferreira, N. J., Silva, M. G. A. J. and Silva Dias, M. A. F. (2009), *Tempo e clima no Brasil*, Oficina de Textos, São Paulo. 463 pp.
- Chao, Y., Farrara, J. D., Schumann, G., Andreadis, K. M. and Moller, D. (2015), Sea surface salinity variability in response to the Congo River discharge, *Continental Shelf Research* 99, 35-45.
- Coles, V. J., Brooks, M. T., Hopkins, J., Stukel, M. R., Yager, P. L. and Hood, R. R. (2013), The pathways and properties of the Amazon River plume in the tropical North Atlantic ocean, *Journal of Geophysical Research: Oceans* 118(12), 6894-6913.
- Dai, A. and Trenberth, K. E. (2002), 'Estimates of freshwater discharge from continents: Latitudinal and seasonal variations', *J. Hydrol.* 3, 660-687.
- Denamiel, C., Budgell, W. P. and Toumi, R. (2013), The Congo river plume: Impact of the forcing on the far-field and near-field dynamics, *Journal of Geophysical Research: Oceans* 118(2), 964-989.
- Eisma, D. and Van Bennekom, A. (1978), 'The Zaire River and estuary and the Zaire outflow in the Atlantic ocean', *Netherlands Journal of Sea Research* 12(3-4), 255-272.
- Foltz, G. R., Schmid, C. and Lumpkin, R. (2015), 'Transport of surface freshwater from the equatorial to the subtropical north Atlantic ocean', *Journal of Physical Oceanography* 45(4), 1086-1102.
- Ffield, A. (2007), Amazon and Orinoco river plumes and nbc rings: bystanders or participants in hurricane events?, *Journal of climate* 20(2), 316-333.
- Foster, R. A., Subramaniam, A. and Zehr, J. P. (2009), Distribution and activity of diazotrophs in the eastern equatorial Atlantic, *Environmental microbiology* 11(4), 741-750.
- Garvine, R. W. (1995), A dynamical system for classifying buoyant coastal discharges, *Cont. Shelf Res.* 13, 1585-1596.

- Garvine, R. W. (1999), Penetration of buoyant coastal discharge onto the continental shelf: A numerical model experiment, *J. Phys. Oceanogr.* 29, 1892-1909.
- Geyer, W. R., Beardsley, R. C., Lentz, S. J., Candela, J., Limeburner, R., Johns, W. E., Castro, B. M. and Soares, I. D. (1996), Physical oceanography of the Amazon shelf, *Cont. Shelf Res.* 16, 575-616.
- Hopkins, J., Lucas, M., Dufau, C., Sutton, M., Stum, J., Lauret, O. and Channelliere, C. (2013), Detection and variability of the Congo River plume from satellite derived sea surface temperature, salinity, ocean colour and sea level, *Remote sensing of environment* 139, 365-385.
- Kerr, Y. H., Waldteufel, P., Wigneron, J.-P., Delwart, S., Cabot, F., Boutin, J., Escorihuela, M.-J., Font, J., Reul, N., Gruhier, C. et al. (2010), 'The SMOS mission: New tool for monitoring key elements of the global water cycle', *Proceedings of the IEEE* 98(5), 666-687.
- Korosov, A., Counillon, F. and Johannessen, J. A. (2015), Monitoring the spreading of the amazon freshwater plume by MODIS, SMOS, AQUARIUS, and TOPAZ, *Journal of Geophysical Research: Oceans* 120(1), 268-283.
- Lentz, S. J. and Limeburner, R. (1995), The Amazon River plume during AMASSEDS: Spatial characteristics and salinity variability, *Journal of Geophysical Research: Oceans* 100(C2), 2355-2375.
- Lentz, S. J. and Largier, J. (2006), The influence of wind forcing on the Chesapeake Bay buoyant coastal current, *J. Phys. Oceanogr.* 36, 1305-1316.
- Masumoto, Y., Sasaki, H., Kagimoto, T., Komori, N., Ishida, A., Sasai, Y., Miyama, T., Motoi, T., Mitsudera, H., Takahashi, K. et al. (2004), A fiftyyear eddy-resolving simulation of the world ocean: Preliminary outcomes of ofes (ogcm for the earth simulator)', *J. Earth Simulator* 1, 35-56.
- Meade, R. H., Rayol, J. M., Da Conceicão, S. C. and Natividade, J. R. (1991), Backwater efects in the Amazon River basin of Brazil, *Environmental Geology* 18(2), 105-114

- Muller-Karger, F. E., McClain, C. R. and Richardson, P. L. (1988), The dispersal of the Amazon's water', *Nature* 333(6168), 56-59.
- Nittrouer, C. A. and DeMaster, D. J. (1996), The Amazon shelf setting: tropical, energetic, and influenced by a large river, *Continental shelf research* 16(5), 553?573.
- Pailler, K., Bourlès, B. and Gouriou, Y. (1999), The barrier layer in the western tropical Atlantic ocean, *Geophysical Research Letters* 26(14), 2069-2072.
- Pimenta, F. M., A. D. Kirwan, J. and Huq, P. (2011), On the transport of buoyant coastal plumes, *J. Phys. Oceanogr.* 41(1), 620-640.
- Pond, S. and Pickard, G. L. (2013), *Introductory dynamical oceanography*, Elsevier.
- Reul, N., Quilfen, Y., Chapron, B., Fournier, S., Kudryavtsev, V. and Sabia, R. (2014), Multisensor observations of the Amazon-Orinoco river plume interactions with hurricanes, *Journal of Geophysical Research: Oceans* 119(12), 8271-8295.
- Signorini, S., Murtugudde, R., McClain, C., Christian, J., Picaut, J. and Busalacchi, A. (1999), Biological and physical signatures in the tropical and subtropical atlantic, *Journal of Geophysical Research: Oceans* 104(C8), 18367-18382.
- Storto, A., Masina, S. and Navarra, A. (2016), Evaluation of the cmcc eddypermitting global ocean physical reanalysis system (C-GLORS, 1982-2012) and its assimilation components, *Quarterly Journal of the Royal Meteorological Society* 142(695), 738-758.
- Stramma, L. and England, M. (1999), On the water masses and mean circulation of the South Atlantic ocean, *J. Geophys. Res.* 104(C9), 20863-20883.
- Wallcraft, A., E. Metzger, and S. Carroll, (2009): Software design description for the hybrid coordinate ocean model (hycom), version 2.2. Tech. rep., NAVAL RESEARCH LAB STENNIS SPACE CENTER MS OCEANOGRAPHY DIV.